Elsevier Editorial System(tm) for Journal of Sound and Vibration
Manuscript Draft

Manuscript Number: JSV-D-07-01447R2

Title: Energy Dissipation Prediction of Particle Dampers

Article Type: Full Length Article

Section/Category: B Passive control of sound and vibration

Keywords: particle damping; energy dissipation

Corresponding Author: Dr. Chian Xng Wong, Ph.D.

Corresponding Author's Institution: University of Sheffield

First Author: Chian X Wong, Ph.D.

Order of Authors: Chian X Wong, Ph.D.; Michelle C Daniel, ; Jem A Rongong, Ph.D.

Manuscript Region of Origin:

Abstract: This paper presents initial work on developing models for predicting particle dampers behaviour using the Discrete Element Method (DEM). In the DEM approach, individual particles are typically represented as elements with mass and rotational inertia. Contacts between particles and with walls are represented using springs, dampers and sliding friction interfaces. In order to use DEM to predict damper behaviour adequately, it is important to identify representative models of the contact conditions. It is particularly important to get the appropriate trade-off between accuracy and computational efficiency as particle dampers □ave so many individual elements. In order to understand appropriate models, experimental work w□s carri□d out to understand interactions between the typically small (~ 1.5-3 mm diameter) particles used. Measurements were made of coefficient of restitution and interface friction. These were used to give an indication of the level of uncertainty that the simplest (linear) models might assume. These data were used to predict energy dissipation in a particle damper via a DEM simulation. The results were compared with that of an experiment.

Energy Dissipation Prediction of Particle Dampers

C X Wong [a,*], M C Daniel [b] and J A Rongong [c].

[a] *Research Associate, Department of Mechanical Engineering, University of Sheffield, Mappin Street, Sheffield U.K., S1 3JD.*

[b] *Student, Department of Mechanical Engineering, University of Sheffield, Mappin Street, Sheffield U.K., S1 3JD.*

[c] *Rolls-Royce Lecturer in Engineering, Department of Mechanical Engineering, University of Sheffield, Mappin Street, Sheffield U.K., S1 3JD*

**Corresponding author. Email:C.X.Wong@shef.ac.uk.*

Keywords: particle damping, energy dissipation

This paper presents initial work on developing models for predicting particle dampers behaviour using the Discrete Element Method (DEM). In the DEM approach, individual particles are typically represented as elements with mass and rotational inertia. Contacts between particles and with walls are represented using springs, dampers and sliding friction interfaces. In order to use DEM to predict damper behaviour adequately, it is important to identify representative models of the contact conditions. It is particularly important to get the appropriate trade-off between accuracy and computational efficiency as particle dampers have so many individual elements. In order to understand appropriate models, experimental work was carried out to understand interactions between the typically small (~ 1.5-3 mm diameter) particles used. Measurements were made of coefficient of restitution and interface friction. These were used to give an indication of the level of uncertainty that the simplest (linear) models might assume. These data were used to predict energy dissipation in a particle damper via a DEM simulation. The results were compared with that of an experiment.

1. Introduction

A particle damper (PD) comprises a granular material (e.g. metallic beads, polymer spheres, ceramic particles etc.) enclosed in a container that is attached to or within a vibrating structure. Vibration energy is dissipated by the damper through inelastic collisions and friction between particles. There is also a momentum exchange mechanism, where momentum is transferred from the primary structure into the particles. This leads to energy storage in the particles in terms of kinetic and strain energy. It is also possible to induce a field of force around the particles (such as filling the enclosures with liquid or applying an electromagnetic field [1]). The main advantage of a particle damper is that its performance does not depend on temperature and can therefore be used

in harsh environments where traditional approaches fail. It also dissipates energy over a range of frequencies not usually encountered in conventional damping solutions.

The concept of PDs is not a product of recent research. In fact, the earliest published work on PDs is thought to have been that of the work of Lieber and Jensen [2] in 1945. In their work, the concept of an acceleration damper was introduced (which in fact is an impact damper, a PD with a single particle) to suppress the aircraft flutter. Other applications of particle damping include the popular Non-Obstructive Particle Damper (NOPD) [3], which introduces damping to a structure by filling particles into voids created within the structure.

Despite the increasing uptake of particle damping technology [4,5,6], the modelling of a particle damper is still complicated by a number of issues. One of the principal challenges in using particle dampers is that they display dramatic amplitude non-linearity – a typical example is presented in Fig. 1 [8]– making them difficult to design. The design problem is compounded by the large number of design parameters, such as the geometry of the enclosure, the material of the particles, the shape of the particles, the packing configuration of the particles, and the application of the field of force around the particles. In order to sidestep these issues, most of the modelling effort has been concentrated in the simplification of the problem, without considering what is happening internally in the PD in detail. An example of such a method is that of modelling the bed of particles as a single effective particle and estimating the performance of the PDs based on this single particle [7]. Other possible methods are to linearise the model for different operating conditions. This was the method taken by Liu and colleagues [8] in estimating an equivalent linear viscous damping coefficient for different levels of excitation. Furthermore, most of these analyses have been conducted within a restricted range of operating conditions, such as that for free decay to equilibrium [9] and for specific sinusoidal frequency excitation [8].Since the damping performance of PDs varies significantly from one operating condition to another, the use of these models is restricted in terms of application.

The parametric models of the simplified approach do not allow one to assign meaningful understanding to the energy dissipation mechanisms of the particle dampers. This is because the dissipation mechanism of the underlying global model is different from one parametric model to the next. While it is possible to calculate the correct dissipated energy from any equivalent model at each operating point it is more satisfactory to extract the information directly from vibration data. One such method is from the Fourier Transform based power flow theory used by Yang [10]. In his application, the average power dissipated (known as active power) and maximum power trapped (known as reactive power) by the vibrating particle damper can be estimated directly via the cross spectrum of the force and response signal of the particle damper. The method is notable for the absence of an attached structure to the particle damper, leading to a greater degree of control in the operating conditions of the particle damper in testing. The power flow method in [10] is, however, a time averaged method and requires the excitation of the damper to be periodic. This is encountered in a large variety of

applications and is sufficient for the purpose of comparison in this paper. Non-periodic power flow can be calculated using more advanced methods, such as the Complex Wavelet Transform [11] which produces the power measurements with localised time-frequency information.

Regardless of the approach to measure or estimate the power dissipation of PDs, the fundamental characteristic that affects the performance of the particle damper is the state of the granular media within the particle damper. Solid, liquid and gas-like phases have been identified for vibrating granular systems [12]. It is due to these analogous properties with molecular gases/liquid, that basic macroscopic fields have been introduced, such as granular temperature, granular velocity and mass density [13]. The granular temperature is simply the ensemble average of the square of the fluctuating velocity of the particles. There are a variety of different definitions of granular temperature in literature, albeit merely scaled versions of the definition mentioned previously [13]. The similarities of flowing granular media to fluid have led to the use of modified hydrodynamic models to explain the behaviour of granular media [14,15]. These are continuum models with hydrodynamic fields with appropriate conservation (conservation of mass, momentum and energy) and constitutive relations (equations that relate stress fields and energy flux to the governing equations). Unfortunately, a simple constitutive relation that can be used for all the three phases of granular media is not available. This is somewhat similar to the case in fluid hydrodynamic models which exhibit different flow regimes, from the standard continuum regime to the Knudsen regime. This has resulted in three main types of constitutive relations based on soil mechanics [16] (for slow plastic flows), Bingham fluid-like visco-plasticity [17] (for intermediate flows with a yield stress and a certain dependence on strain rate) and statistical mechanic kinetic theory [14] (for granular gas where friction is largely ignored). A mix of all three has been attempted as well, with some degree of success [18].

The biggest advantage of the hydrodynamic approach is that it has, surprisingly, managed to predict certain granular flow behaviour despite the exclusion of explicit particle level dynamics. However, limitations to the models are certain to exist due to prior assumptions made in the construction of the hydrodynamic models [13]. For example, the assumptions of molecular chaos (no correlation of position between particles), equipartition (equal levels of energy in each degree of freedom), Maxwell-Boltzmann distribution (3-dimension Gaussian distribution of particle velocities) are broken in strongly vibrated granular media. These assumptions are the foundation of the kinetic theory used in the construction of hydrodynamic models. The slow plastic flows and intermediate flows are also dependent on a measurement of bulk properties from experiments. However, the particle level dynamics (microscopic in terms of molecular gas/fluid) can become dominant in certain situations, especially when particles with different properties are within the granular media. This lack of scale separation between microscopic and macroscopic properties can lead to wildly different calculated values as hydrodynamic models are mostly dependent on the “box-division” method to estimate field values [13].

It appears that the only way to get the best predictions is to simulate the media at the most fundamental level, the particle level. Particle level dynamics simulation has been studied under different names such as Discrete Element Modelling (DEM) and Molecular Dynamic (MD) simulations. In recent years, DEM has been used increasingly to model granular media. This is due to the rapid improvements in computational hardware and software over the years. It may well be that the computational burden of hydrodynamic or hybrid DEM/hydrodynamic models are still much lower than pure DEM simulations. However, the trade-off between particle level resolution and computational costs are becoming less of an issue with time. Creating models that are physically sound in the hydrodynamic approach is also non-trivial, whereas DEM-based approaches rely on simple parameters that can be acquired in a simpler manner.

Particle dynamics simulation methods are usually divided into two categories, hard sphere and soft sphere models. The hard sphere models do not rely on the modelling of complex contact mechanics. Usually, the only needed properties are the coefficient of restitution, α (the ratio of rebound momentum to impact momentum) of particle-particle collision and particle-wall collision, the mass and size of the particles. The simulation time step is variable and each time step represents a new collision. Therefore, it is also known as the Event-Driven simulation method [19] as it only records collision events and nothing between collisions. Obviously the absence of deformation mechanics allows this method to be executed quickly for a large number of particles, though oversimplification of deformation mechanics removes information that can be helpful for the design of particle dampers. Hard sphere models are also plagued by problems of inelastic collapse [13]. Recall that since there is no compliance, particles rebound immediately when collision occurs, irrespective of the collision velocity. Consider a system where a particle collides with a cluster of particles. In the case of elastic collisions, the cluster may break up and the subsequent time steps get larger before each collision event. In a system where the coefficient of restitution of a particle is less than 1 (inelastic), the impacting particle may rebound wildly within the cluster as it reaches equilibrium, where the collision distance and time step for each subsequent collision gets shorter. This leads to near infinite collisions in a finite time, which may sometimes result in a string of particles appearing stationary while many time steps have passed in the simulation. This is a numerical problem and should not be confused with “clustering”, a real phenomena where a high number of inelastic collisions in a cluster leads to the growth of the cluster and the average temperature of the cluster.

Soft sphere models [20], like the hard sphere models, involve individual particles which are typically represented as elements with mass and rotational inertia. They differ from the hard sphere models however, by allowing the particles to overlap. The contacts between particles and with walls are usually represented using springs and sliding friction interfaces. In commercial DEM software, contact conditions can be specified to different levels of complexity. A linear spring is the simplest representation of contact stiffness with the next simplest being Hertz-Mindlin force-displacement behaviour [20] (a nonlinear formulation where the contact force follows a power law). Similarly, the simplest models for representing energy loss mechanisms include

simple viscous, hysteretic and Coulomb models. In order to use DEM to predict damper behaviour adequately, it is important to identify representative models of the contact conditions. It is particularly important to get the appropriate trade-off between accuracy and computational efficiency as particle dampers have so many individual elements. Ideally, one would prefer the simplest model possible while minimizing the loss of accuracy of the models. Some work on the characterization of particle damping in free decay vibrations has been attempted using these soft sphere models [21].

Most of the hydrodynamic models devised so far have been compared to models simulated using DEM. This is due to the great difficulty in acquiring reliable experimental results. The best validation of results should come from the measurement of the state up to the particle level. In recent years, researchers are only beginning to tap into new experimental techniques, such as Position Emission Particle Tracking (PEPT) [22] for particle tracking. In the interest of this paper however, the power dissipation measurement is considered sufficient for the purposes of comparison. In order to understand appropriate models, experimental work was carried out to understand interactions between the typically small (~ 1.5-3 mm diameter) particles used. Simple measurements were made of coefficient of restitution and interface friction. These data were used to predict energy dissipation in a particle damper via a soft sphere DEM simulation.

Section 2 of the paper details the contact models and simulation variables used in the DEM simulation. Section 3 of the paper relates the different experiments performed to estimate the friction and impact damping of the particles. Section 4 relates the comparison between power dissipation measured in a forced vibration experiment and those simulated in DEM. The paper is concluded in Section 5.

2. The Discrete Element Method

The 3-dimensional discrete element method used here is based on the commercial software, PFC3D 3.1 [23]. The details of the method can be found in reference [23]. A brief review is mentioned here for completeness. In this implementation, all the particles are assumed to be perfect spheres (although clumps can be bonded together to form irregular particles). The particles are also assumed to be rigid, and the particle displacement and contact area small relative to the particle sizes.

The equations of motion are applied for each particle, based on the resultant force and resultant moment on each particle. Laws of motion are not applied to the walls in the simulation. The motion of walls however is explicitly controlled utilizing a specified wall velocity as an input. The equations of motion for the *i*-th particle in vector form are given as:

$$\mathbf{F}_i = m_i(\ddot{\mathbf{x}}_i - \mathbf{g}_i) \tag{1}$$

$$\mathbf{M}_i = \left(\frac{2}{5} m_i R_i^{\,2}\right)\dot{\boldsymbol{\omega}}_i \tag{2}$$

where $\mathbf{F}_i$ is the resultant force vector, m_i is the mass of i-th particle, $\mathbf{x}_i$ is the position vector of the particle, $\mathbf{g}_i$ is the body acceleration vector (e.g. gravity), R is the particle radius, $\mathbf{M}_i$ is the resultant moment and $\boldsymbol{\omega}_i$ is the angular velocity vector. The dot above the variables represents the derivatives of the variables with respect to time. Given the resultant forces and moments, the position of the particle in one time step, Δt, is updated based on the equation:

$$\mathbf{x}_i^{\,(t+\Delta t)} = \mathbf{x}_i^{\,(t)} + \dot{\mathbf{x}}_i^{\,(t+\Delta t/2)}\Delta t \tag{3}$$

where the mid interval quantities are computed based on a centred finite difference scheme of the velocities:

$$\dot{\mathbf{x}}_i^{\,(t+\Delta t/2)} = \dot{\mathbf{x}}_i^{\,(t-\Delta t/2)} + \left(\frac{\mathbf{F}_i^{\,(t)}}{m_i} + \mathbf{g}_i\right)\Delta t \tag{4}$$

$$\boldsymbol{\omega}_i^{\,(t+\Delta t/2)} = \boldsymbol{\omega}_i^{\,(t-\Delta t/2)} + \left(\frac{5\mathbf{M}_i^{\,(t)}}{2m_i R_i^{\,2}}\right)\Delta t \tag{5}$$

For a multi-particle system, a critical time step value is chosen automatically at each iteration step. The critical time step is related to the highest natural frequency in the system. To perform a global eigenvalue analysis of the system is expensive. Therefore a simplified approach is used to estimate the critical time step. A simple analysis of an uncoupled multi-degree-of-freedom system of linear springs and masses lead to a critical time step:

$$t_{\text{crit}} = \min\begin{Bmatrix}\sqrt{m_{\min}/k^{\text{tran}}} \\ \sqrt{I_{\min}/k^{\text{rot}}}\end{Bmatrix} \tag{6}$$

where I_{min} is the smallest moment of inertia in the system, m_{min} is the smallest mass in the system, k^{tran} is the highest effective translational stiffness from every degree-of-freedom and k^{rot} is the highest effective rotational stiffness from every degree-of-freedom.

The time step chosen in simulation is actually the critical time step multiplied with a safety factor, SF. The safety factor is fixed at 0.8 in this work.

The resultant forces and moments can be decomposed to the shear and normal forces acting on the particles. This relates to the force-displacement contact laws. For a small area of contact between two nonconforming bodies with an elliptical profile, the elastic regime of a normal contact can be modelled using the well known Hertzian contact [24]. The Hertzian contact relates a nonlinear normal force as the function of normal displacement, δ_n:

$$f(\delta_n) = \frac{4}{3} E^* R^{*1/2} \delta_n^{\,3/2} \tag{7}$$

where E^* is the effective Young's Modulus:

$$\frac{1}{E^*} = \frac{1-\nu_1^{\,2}}{E_1} + \frac{1-\nu_2^{\,2}}{E_2} \tag{8}$$

E_1 and E_2 are the Young's Modulus while ν_1 and ν_2 are the Poisson's ratio of the two contacting bodies. R^* is the effective radius of the two contacting bodies 1 and 2:

$$\frac{1}{R^*} = \frac{1}{R_1} + \frac{1}{R_2} \tag{9}$$

The radius of contact area, ϕ_i for a particle contact on a rigid half-space is related to the normal displacement by the equation:

$$\phi_i = \sqrt{\delta_n R_i} \tag{10}$$

For small contact area, the Hertzian model can be used for contact between particles and between the particles and the wall. Unfortunately, there are a number of shortcomings with a pure Hertzian model.

First of all, it is only valid for the elastic regime. Some sort of plastic deformation is expected for certain operating conditions of the particle dampers. This would lead to a decrease in overall stiffness when regions of the particles start to become plastic. Constitutive equations that relate the force-displacement law for the three different regimes (elastic, elastic-plastic and fully plastic) do exist for collisions between similar particles [25]. However these relations are discontinuous and non-Hertzian elastic contacts (which exist in collisions between dissimilar particles) would reduce the usefulness of these relations. Nevertheless, some sort of simplification is needed in order to make the calculations tractable. Therefore, the constitutive relations of [25] are still a good candidate to approximate the contact behaviour. There are, however, other problems with the Hertzian model that are numerical in nature.

From Eq. (6), it is known that the critical time step is inversely proportional to the effective stiffness. Particles with high stiffness require a larger number of time steps to reach a certain point in time. From the Hertzian relationship in Eq. (7), the effective stiffness of a particle can rapidly change with increasing displacements (due to the power term). In a Hertzian model undergoing compression, a much smaller time step is needed than the critical time step calculated at the current point in order to maintain stability. However, it is not trivial to estimate this new critical time step. A possible solution is to select a much smaller safety factor, say 0.3. In this work however, the elastic portion is modelled using a linear spring. This alleviates the problem of selecting an appropriate critical time step and speeds up the simulation significantly. To assign the correct stiffness value to the linear spring, Coaplen and colleagues suggested an equivalent linear spring that would store the same amount of energy up to a similar yield force for a Hertzian model [26]. By integrating Eq. (7) up to the yield displacement, δ_{ny} , one would acquire the energy stored up to the yield point as:

$$W_y = \frac{2}{5} f_y \delta_{ny} \tag{11}$$

where f_y is the normal yield force. The equivalent energy stored for an equivalent linear spring model up to the yield force is given as:

$$W_y = \frac{1}{2} k_{\text{eq}} \left(\frac{f_y}{k_{\text{eq}}} \right)^2 = \frac{1}{2} \frac{{f_y}^2}{k_{\text{eq}}} \tag{12}$$

The mean contact pressure to initiate yielding for spherical contact surfaces was found to be $1.1Y_i$ [24], where Y_i is the yield stress of the *i*-th particle. This relates to contact radius of equation (10) by:

$$\frac{f_y}{\pi {\phi_i}^2} = 1.1Y_i \tag{13}$$

Combining Eqs. (11), (12) and (13), we arrive at the equivalent stiffness of the particular body in consideration:

$$k_{ni} = \frac{5.5}{4} \pi Y_i R_i \tag{14}$$

where Y_i is the yield stress for the body in consideration. It is assumed that a large proportion of the collisions would be slightly inelastic collisions. If this assumption holds true, the average normal contact stiffness should be close to that given in Eq. (14).

In an earlier work prior to this publication [27], it was assumed that the tangential stiffness played a negligible role in terms of energy storage and in energy dissipation. The tangential stiffness was then selected to be the same as the normal stiffness for simplicity. In this work, the validity of this assumption is evaluated by comparing it to simplified linear models of the existing complicated nonlinear models for shear interactions between particles. The Mindlin-Deresiewicz [28] model is an example of such a model and is given as:

$$\Delta T = 8G^* \theta_k \phi \delta_s + (-1)^k \mu f(\delta_n)(1 - \theta_k) \tag{15}$$

where ΔT is the incremental tangential force, δ_s is the shear displacement, μ is the friction of coefficient and G^* is the reduced shear modulus given by:

$$\frac{1}{G^*} = \frac{1 - {\nu_1}^2}{G_1} + \frac{1 - {\nu_2}^2}{G_2} \tag{16}$$

where G_1 and G_2 are the shear modulus of the two contacting bodies. The parameter θ_k depends on which portion of the cycle of loading it is on. It is given as:

$$\theta_k = 1 \text{ if } |\Delta T| < \mu f(\delta_n) \text{ for no-slip} \tag{17}$$

otherwise:

$$\theta_k = \sqrt[3]{1 - \frac{T + \mu f(\delta_n)}{\mu f(\delta_n)}} \text{ if } k = 0 \tag{18}$$

$$\theta_k = \sqrt[3]{1 - \frac{(-1)^k (T - T_k) + 2\mu f(\delta_n)}{2\mu f(\delta_n)}} \text{ if } k = 1,2 \tag{19}$$

where k = 0, 1 and 2 represents the loading path, unloading and reloading, respectively. It is noted that this formulation involves the friction characteristics of the contacts, where μ is the friction coefficient. There is also the presence of memory in the system with the inclusion of T_k, which is the tangential force at which loading or reloading begins. To extract a linearised version of a constant tangential stiffness, certain assumptions were made. The radius of the contact area is set as a constant and at the value where yield initiates during compression. The material was also assumed to be isotropic. Utilising Eq. (7) and Eq. (13), the tangential stiffness is acquired from the no-slip solution of the Mindlin-Deresiewicz model (Eq. (15)):

$$k_{si} = \frac{3.3}{(1+\nu)} \pi Y_i R_i \tag{20}$$

The friction dissipation in the shear direction is also separated into an independent formulation, namely Coulomb friction:

$$f_{\text{Coulomb}} = \mu f(\delta_n) \tag{21}$$

For typical metals, the Poisson's ratio is around 0.3. This yields a tangential stiffness of roughly 1.8 times the normal stiffness. The scale of the tangential stiffness is therefore very close to the normal stiffness and the assumptions made in the previous work is somewhat justified. The memory elements of the Mindlin-Deresiewicz model have also almost completely been eliminated by the replacement of the continuous nonlinear friction portion of the original formulation with the Coulomb slider. It is possible to reintroduce some elements of the memory back into the system via a shear viscous damper. However, the memory introduced would not be non-local like the Mindlin-Deresiewicz formulation (where the memory presence is different depending on the loading cycle). The shear viscous damper is neglected in the subsequent simulations for simplicity, though it might be useful in future works for model tuning.

So far nothing has been mentioned on the collision damping mechanisms of the particle. In order to simulate the plastic deformation in normal contacts, viscous damping is added to the particles. This actually does not relate to real plastic deformation as plastic deformation is rate independent [26]. However, it is something that is easily implemented in a simulation and is commonly used in other DEM works [21]. The coefficient of restitution, α can be related to the critical damping ratio, ζ by [29]:

$$\zeta = \frac{\ln(\alpha)}{\sqrt{\ln^2(\alpha) + \pi^2}} \tag{22}$$

In fact it appears that α varies with impact velocity [30]. Actually this is just the manifestation of the transition from an elastic collision to a pure plastic regime. Therefore, it is actually independent of velocity and is dependent on the work done on the particle in compression. Coaplen [26] discusses the energetic definitions of the coefficient of restitution and how α should be measured in energy terms as a general model for collisions of any type (including dissimilar particles). In this work however, a constant value of α is used throughout the simulations.

The normal viscous damping coefficient (the viscous damping is a function of contacts, not of entities) is then set as:

$$c_n = 2\zeta\sqrt{k_n m^*} \tag{23}$$

where ζ is the critical damping ratio and k_n is the effective normal stiffness of the two contacting bodies. m^* for a ball-wall contact is simply the mass of the ball, while for a ball-ball contact, it is given as:

$$\frac{1}{m^*} = \frac{1}{m_1} + \frac{1}{m_2} \tag{24}$$

where the m_1 and m_2 are the mass of the two balls that are in contact.

For a system with viscous damping, the timestep is reduced further by a correction factor to the effective stiffnesses [31]. The effective stiffnesses for each degree-of-freedom are a function of the tangential and normal stiffnesses, and are corrected via:

$$k'_{n/s} = \kappa \frac{k_{n/s}}{\left(\sqrt{1+\lambda_{n/s}{}^2} - \lambda_{n/s}\right)^2} \tag{25}$$

where $k_{n/s}$ are the original normal/tangential stiffnesses, $k'_{n/s}$ are the corrected stiffnesses, κ is a safety factor, while $\lambda_{n/s}$ is given as:

$$\lambda_{n/s} = \frac{c_{n/s}}{2k_{n/s}\Delta t_0} \tag{26}$$

$c_{n/s}$ is the damping coefficient in the normal and tangential direction, while Δt_0 is the timestep for the system without viscous damping. A diagram of the contact models for different collisional conditions is shown in Fig. 2. The stiffness of the contacting entities are actually the effective stiffness (equivalent spring for two springs connected in series) while the coefficient of viscous damping can be found from a derivation of Eq. (23).

The yield strength of the materials that are required to calculate the values of stiffness for the contacts are well documented in literature. The other two key parameters, the coefficient of restitution and the coefficient of friction, need to be determined from experiments. Note that these are properties of contacts, not of entities. Simple experiments were conducted to extract this information. The results of the experiments are detailed in the next section.

3. Experimental Characterization of Contact Properties

A variety of different particles were tested to acquire approximate values of the coefficient of friction and the coefficient of restitution. These range from 0.6 mm diameter steel shot, chrome ball bearings (sizes 1.5, 2.0, 2.5, 3.0 mm diameter) and stainless steel ball bearings (sizes 1.5, 2.0, 2.5, 3.0 mm diameter).

Two different types of material surfaces were also tested (stainless steel and Perspex), as these are popular materials used for constructing particle damper casings.

3.1. Identification of Coefficient of Friction

The coefficient of friction was identified using a traditional one-direction sliding friction rig. Fig. 3 shows the sliding plate friction rig which was chosen to collect the friction data.

The spherical particles used in this test were attached to small (20x20x3mm) steel plates using rigid epoxy adhesive and left to set. Strong double sided adhesive tape was used to attach these plates individually to the moving arm on the rig (refer to Fig. 3). The arm pivots, allowing the particle(s) to rest on the surface of the test plate, which is itself attached to the sliding plate on the rig. Test plates were made from Perspex and stainless steel. In the case of the steel plates, sliding with the grain and against the grain was considered separately. Before testing, particles and test plates were cleaned with degreaser. When the rig is switched on the plate starts to move, forcing the arm to compress the load cell. The force that the load cell measures is proportional to the friction force. For this experiment the particles were positioned 95mm from the pivot while the load cell was 35mm away. From moment calculations therefore, the friction force is around 37 percent of the force applied to the load cell.

To obtain the friction coefficient from the friction force, the normal load on the specimen/plate contact point is required. The normal load was acquired by placing a calibrated load cell on the plate at the point where the particle makes contact. The height of the arm was altered so that the arm was level on contact. This force was measured 25 times and the mean was taken to be 0.5167N. This is equivalent to approximately 1.4 metres of 3mm stainless steel ball bearings resting on top. At low loading levels, the normal load should not affect the friction coefficient. In order to check this assumption, results obtained for mono-particle and multi-particle contacts for the same load condition were tested.

Testing was carried out at a number of different sliding speeds. The instantaneous value of the coefficient of friction was calculated and recorded in real-time. The time trace resulting from a typical test is presented in Fig. 4. On this plot, transients from the initial start-up can be seen around 4 seconds while steady state behaviour is

assumed after 5 seconds. The coefficient of friction was taken, in each case, as the time-averaged, steady state value of the instantaneous measurement.

Fig. 5 shows the results of tests over a range of speeds for both the single particle and the multiple particle conditions. The variability in test results, up to approximately 20%, is typical of the level of reproducibility identified during these tests. From the trend lines, it can be seen that the coefficient of friction increases with velocity – a feature that has been reported in some cases in literature [32] and is attributed to the inertia of the asperities in contact (for dry friction) and viscous damping (in lubricated surfaces). It is unclear at the moment whether these effects will be replicated in a particle damper. In case it should manifest itself, the model involving the shear viscous damper, mentioned in Section 2, might be a useful approximator. Nevertheless, these effects are currently ignored during modelling. It can also be seen from Fig. 5 that there is little difference in results obtained from the multiple particle and single particle test results. Because of this, subsequent tests involved the single particle format as it was easier to fabricate and control. Tests were repeated 18 times per particle type over 2 different speed settings. The mean results are given in Table 1. Note that the test plate was moved sideways after each test to ensure that the subsequent test involved contact between surfaces that had not previously been in contact.

As noted earlier, examination of Table 1 shows that the results display significant scatter. This is not surprising as it is well known that tiny imperfections or irregularities to the surface can have a major effect on the friction coefficient. The imperfections could be small surface scratches or irregularities on the plate, tiny amounts of surface dust or rust, grease or oxidised surfaces. While the spread of results may be decreased by carrying out more extensive surface treatment and cleaning prior to testing, the results obtained from these tests are arguably more valuable in that they show the variability in coefficient of friction that might be expected in a real particle damper. It is interesting to note that the direction of sliding on the same metal surface can alter the results by more than 20 % in some cases.

Future tests with a smaller normal load would be useful to ensure that the friction coefficients obtained are similar to those obtained in these experiments. Smaller normal loads could be achieved by hanging weights off the opposite end of the arm to the test specimen to act as a counter balance. Also it would be useful to show whether the friction coefficient at the bottom of a particle damper are similar to that of those particles near the top. The current results however are considered sufficient for the work presented here.

While particle-plate friction is relatively easy to measure, this is not the case for particle-particle friction. Existing methods based on rotary rigs are more suitable for higher sliding velocities than those expected in particle dampers. Instead, in this work, the particle-particle coefficient of friction is assumed to be the same as for the particle-plate contact. The justification for this assumption is twofold. First, as the scatter in measured

values is quite large it may hide any differences. Second, the work of Li and colleagues [33], presents a reasonable physics-based argument for the assumption. They state that as the area of a particle-particle contact is so small it can be considered a point contact and the area of a plate-particle contact is also so small it can be considered a point contact. Therefore, Li declares that for small particles, the friction coefficient of a particle-particle contact is the same or very similar to that of a particle-plate contact, when the plate is made from the same material as the particle and has the same surface conditions.

3.2. Identification of Coefficient of Restitution

Two simple sets of experiments were performed to identify the coefficient of restitution; a particle-particle collision test using a pendulum and a particle-wall test using a drop test rig.

In the particle-particle collision test, a makeshift pendulum (a variant of the Newton's Cradle) was set up. Diagrams of the set up are shown on Fig. 6 and Fig. 7.

Each ball bearing marked for testing was cleaned and bonded to the middle of a long (~0.5m) piece of 0.052mm diameter nylon fishing line using ceramic adhesive. Once the adhesive dried, the test ball bearings were suspended from a raised beam for 24 hours to allow for any wire creep deformation from the weight of the ball.

After this 24 hour period, two ball bearings were suspended and aligned as shown in Figs. 6 and 7. The alignment of the two particles was achieved by marking two points 144mm apart and hanging a plumb line from the centre point verifying the true vertical centre point. The wires suspending Ball 1 were attached to the marked points using double-sided adhesive tape and their heights were adjusted until Ball 1 was aligned with the plumb line. Ball 1 was fixed at this position. The wires suspending Ball 2 were then taped to the marked points and their heights adjusted until they aligned with Ball 1. This alignment was only judged by the human eye and results would improve with a more accurate method.

A vacuum pump with a nozzle was used to release Ball 1. The tip of a click pencil made an excellent nozzle. This was attached to the vacuum pump tube using a thinner inner tube. Small air release holes were added to the inner tube using a pin so that when the pump was switched off the suction pressure would diminish and the ball would be released.

The vacuum pump nozzle was held in place using a clamp and stand. The height (y position) was adjusted to a desired height above the balls in neutral position. The x and z position of the nozzle could then be adjusted to hold Ball 1 in its equilibrium trajectory.

A high speed video camera was used to capture the particle drop, collision and rebound. The camera was set up to record at 900 fps in a 512mm x 128mm resolution area. Two or three flood lights were required to provide enough light to capture the image, however, it was important not to position these too close to the suspension wires or to leave them on between tests as excess heat from the lights leads to thermal plastic deformation of the wires.

The stainless steel ball bearings were captured best with a black background, but due to the brown/orange colour of the chrome ball bearings, these were captured best with a white background.

The release height was varied and at each height 5 repeats were taken. Coefficients of restitution were found for the initial collision and the rebound collision; any collisions after this were classed invalid for finding the coefficient of restitution because the lower ball about to be impacted was still moving. Note that for all the tests, the impacting ball was almost stationary post collision.

An x and y pixel to distance reference was taken for each test by capturing a ruler. If the camera is adjusted, the reference becomes invalid and a new reference must be taken. The reference is then used to calculate the pixel to meter conversion factor.

The coefficients of restitution of the tests were found by calculating the ratio of the rebound height of the impacted ball bearing and the initial height of the impacting ball bearing. No corrections were made to account for the rebound height of the impacting ball bearing as this was assumed stationary. Some results of the experiment are shown in Fig. 8.

It can be see that the coefficient of restitution calculated from the initial impact differs from the rebound collisions. This is thought to be partially due to the stationary assumption made on the impacting ball post collision. There is also the chance that the collision is not strictly collinear due to small inaccuracies in initial alignment. It can be seen however, that the coefficient of restitution of the initial impact actually increases with impact velocity. This seems to contradict what is normally expected as higher velocities correlates with more work done to deform the balls plastically, which would result in lower coefficients of restitution. It is therefore, not possible to garner anything conclusive from the results of both impact conditions, although the rebound impact measurements are nominally more feasible. Nevertheless, the range of values of the coefficient of restitution, between 0.8-0.95, compares fairly well with other values found in literature [30].

The drop test rig was used to characterize the coefficient of restitution between the particles and the wall. The basic drop test rig used is shown in Fig. 9. A vacuum pump with a nozzle was used to release the test ball from various selected heights, h_0. The tip of a click pencil was used as the nozzle except for releasing the 0.6mm

steel shot, which were too small, so a smaller nozzle was produced from cardboard for these particles. This was attached to the vacuum pump tube using a thinner inner tube. Small air release holes were added to the inner tube using a pin, so that when the pump was switched off, the suction pressure would diminish and the ball would release. When released the test particle hits and rebounds off a stiff test plate several times. In this case the plates tested were made of Perspex (100x75x19mm) and stainless steel (100x100x20mm).

A piezoelectric transducer (PZT) pad was mounted to the base of the test plate using ceramic glue. The sampling rate and sensitivity were adjusted to produce a clear, detailed time history of the impacts acquired from the PZT. The impact force time history was used to find the time interval between two successive collisions, t_m, which was used to calculate the coefficient of restitution:

$$\alpha = (g/8h_o)^{1/2} t_m \tag{27}$$

where h_0 is the height before the collision and g being the gravity acceleration constant. Velocity of impacts was calculated based on the equation:

$$v = (2gh_0)^{1/2} \tag{28}$$

Results of various coefficients of restitution of particle-wall contacts are shown in Fig. 10 and Fig. 11. The coefficient of restitution values are roughly similar for different particles, suggesting that the property is mostly dominated by the property of the wall.

4. Experiment Verification and Simulation of Particle Dampers

4.1. Power Measurement Experiment

A Perspex particle damper was chosen for the characterization procedure. This is similar in construction to the particle damper used by Yang [10]. The particle damper consists of a cylindrical casing with a screw top lid and a securing ring. The screw top lid allows the attenuation of the distance between the top layer of the particles and the bottom of the casing lid. The transparent casing also allows one to view the movement of the particles during the operation of the damper. A schematic of the particle damper is shown in Fig. 12 while a picture of the particle damper test setup is shown in Fig. 13.

In order to verify the simulation, power dissipation measurement tests were conducted on the particle damper. This is based on the Fourier based power flow method that Yang [10] used to characterize particle dampers. Basically, it is known that work done in a cycle to excite a mass is given as:

$$W_{cycle} = \int_0^T f(t)v(t)dt \tag{29}$$

where $f(t)$ and $v(t)$ are the force and velocity respectively and T being the length of one cycle. The term $f(t)v(t)$ is denoted as the instantaneous power. The average power transmitted is therefore given as:

$$P_{av} = \frac{W_{cycle}}{T} = \frac{1}{T}\int_0^T f(t)v(t)dt \tag{30}$$

Eq. (30) can be easily interpreted as an average of instantaneous power. If the force and velocity dataset is represented as a complex Fourier series in a discrete manner (with the real values represented in the real portion of the Fourier series), one arrives at the equation:

$$P_c = \frac{1}{T}\int_0^T \left(\sum_{n=0}^{\infty} f_n e^{j(n\omega t-\alpha_n)}\right)\left(\sum_{n=0}^{\infty} v_m e^{j(m\omega t-\beta_m)}\right)dt \tag{31}$$

where P_c is the complex power ; f_n and v_m are the magnitude of the force and velocity of the n-th and m-th harmonic respectively; e is the Euler number; j is the imaginary number; ω is the fundamental frequency in rad/s; and α_n and β_m are the phase of the force and velocity of the n-th and m-th harmonic respectively. Due to the orthogonality of harmonics, the integrals between all cross-terms cancel out:

$$P_c = \frac{1}{2}\sum_{n=0}^{\infty} f_n v_n e^{j(\alpha_n-\beta_n)} \tag{32}$$

The average dissipated power (also known as active power in electrical engineering) can be extracted from the real part of the complex power. The imaginary part of Eq. (32) corresponds to a term usually known as reactive power (also a term borrowed from electrical engineering). Reactive power is conventionally interpreted physically as the maximum power stored in the system. The derivation of reactive power comes from the phasor

difference between apparent power (the product of root-mean-square of force with the root-mean-square of velocity) and active power.

The complex power can be easily acquired from experiments via the cross-spectrum calculation built-in in most signal analyzers. The complex power spectrum for the *n*-th harmonic is given as:

$$P_n = f_{n,rms} v^*_{n,rms} \tag{33}$$

where $f_{n,rms}$ denote the Fourier transform of the force normalized to its root-mean-square level (dividing the magnitude by $\sqrt{2}$); while $v^*_{n,rms}$ is conjugate of the Fourier transform of the velocity normalized to its root-mean-square level. The total complex power, P_c is the sum of the complex power spectrum over all the harmonics:

$$P_{complex} = \sum_n P_n \tag{34}$$

It is possible to perform the same power measurements for any signals using this method, provided that it is a periodic signal. Vibration damping however is usually analysed within single resonances. Therefore, analysis in this work has been restricted to the use of single harmonics. This would result in analysis being restricted to Eq. (33). For complicated structures with multiple resonances, the analysis may be repeated to account for the different resonances.

One of the popular methods to measure the damping efficiency of materials is via the use of the damping loss factor. This is given as:

$$\begin{aligned} \eta &= \frac{\text{Energy dissipated in a cycle per radian}}{\text{Maximum energy stored in a cycle}} \\ &= \frac{\text{active power}}{\text{reactive power}} = \frac{\text{Re}\{P_n\}}{\text{Im}\{P_n\}} \end{aligned} \tag{35}$$

Particle dampers can be used in two ways; as a separate attachment to the structure to mitigate vibration or built-in into the system by filling voids within the structure with the particles. The latter method is attractive as it avoids adding additional mass to the structure externally, resulting in space savings and perhaps even reducing the weight of the overall structure. In this work however, we are more particularly concerned about the

use of the particle damper as a separate attachment. By using it as an attachment, the particle dampers are likely to be much lighter than the weight of the overall structure. This is because attachments are usually a “quick-fix” solution for an existing design. The original structure was not designed to take additional mass so adding too much mass may lead to other structural problems, not to mention possible additional transportation costs. The maximum energy stored by the particle dampers are therefore negligible compared to the energy stored in the vibrating structure. The primary form of vibration suppression is therefore assumed to come from the energy dissipation mechanisms, rather than momentum transfer and subsequent storage of energy in the particles in terms of kinetic and strain energy. The energy dissipation measurements should also hold constant for the same operating conditions regardless of the structure it is attached to. It is convenient though to produce some plots of the loss factor to get an idea of how effective particle dampers are, if we consider it as an energy dissipating material. Further work to identify whether momentum transfer mechanisms can be exploited for vibration attenuation will be performed in the future.

Initially, four different sets of experiments were conducted to characterize the damper; vertical stepped-sine test with 225 stainless steel ball bearings of 3mm diameter, 389 stainless steel ball bearings of 2.5 mm diameter, 760 stainless steel ball bearings of 2mm diameter and 1800 stainless steel ball bearings of 1.5 mm diameter. All of the stepped sine tests were performed at frequencies of 45 Hz, 65 Hz and 85 Hz over excitation amplitudes of 5g, 7g, 9g, 11g and 13g with the height of the lid from the base fixed at 30 mm. The tests involve mounting the Perspex damper onto an electromagnetic shaker. The connection between the PD and the shaker is buffered by a force transducer, while the response of the damper is measured with an accelerometer (which is integrated to retrieve the velocity). The analysis was deliberately restricted to stainless steel ball bearings to simplify the comparison procedure. The number of particles was also deliberately chosen in such a way to ensure the overall mass from one set to the next is exactly the same.

The use of this technique comes with a few caveats. First of all, the excitation is assumed to be perfectly sinusoidal. Although easily achieved in simulation, it is not so in the case of experiments. The voltage passed into the electrodynamic shaker may be sinusoidal, but the velocity measured is rarely a perfect sinusoid. The second assumption made in this method was that the walls were rigid, at least externally. This problem is however less significant as it is intertwined with another, measurement phase lags. The measurement of signals from experiments with an empty casing exhibits a phase lag in measurement. This is more of an electronic phase error of the signals, though part of the phase error might originate from the rigid casing assumption. This problem was also encountered by Yang [10] and should be compensated to avoid potential large measurement errors. One only has to perform the power measurement experiment with an empty particle damper casing and take note of the phase lag. This phase should be added to the phase difference of subsequent experiments with the particles.

5. DEM simulations

Appropriate values of parameters are needed to simulate the initial sets of experiments. First of all, the yield strength of stainless steel is needed to estimate the linear contact stiffness of the particle. An approximate value acquired from data handbooks is given as 345 x 10^6 Pa. Data handbooks also give a density of stainless steel as 7800 kg/m^3. This is needed to calculate the mass of the particles. The coefficient of restitution for both particle-wall and particle-particle contacts is chosen as 0.92. This is the average value acquired for the stainless steel ball bearings colliding with one another and with a Perspex wall. It was also assumed that contact between the stainless steel test plate and the stainless steel ball bearings used in the sliding friction rig is roughly the same conditions as that between the ball bearings. This is somewhat justified by the point contact as described in Section 3. This would lead to a value of around 0.4 for the coefficient of friction for both particle-wall and particle-particle contact.

Having chosen the required values, models of the Perspex PD can now be created. First of all, the walls (assumed rigid) of the PD are created. Particles are then randomly generated within the walls. The particles are then allowed to fall from gravity loading and to settle within 60,000 time steps. The walls are then excited in a sinusoidal fashion for 150,000 time steps. 75,000 time steps of work done by the walls were recorded (by downsampling the 150,000 time steps to reduce storage space) at the end of each run. A typical example of the process involved in modelling is shown in Fig. 14.

Due to the energy balance, the steady state work done by the walls is equivalent to the energy dissipated by damping. The first 20,000 time steps of the energy trace recorded were deleted to remove the transients. The remaining values were then used to estimate the power dissipation by fitting a linear model to the time history. Comparisons between the power dissipation measured from the experiments and that of the simulation are shown in Fig. 15.

It can be seen that despite all the simplifications made so far, the results match within the same scales with the experiments. The only glaring exceptions are that for high amplitude excitations for the 3 mm diameter ball bearings and that of the highest and lowest amplitude excitation of the 1.5 mm diameter ball bearings. It is thought that some of this mismatch could be due to the problem of transients.

Although care has been taken to exclude the earlier time history to remove transients, one does not know a priori how long the system would take to settle. It varies a lot from one system to another. This transient is present because it takes time for the vibrating damper to break up the clumps of particles. An example of such a clump that acts as a bulk can be seen in Fig.14(c). Identifying the transient behaviour from visual clues can be

cumbersome. A better indicator may be in the energy trace. A typical plot of an energy trace that has been plagued by the transient problem is shown in Fig. 16 (a).

It can clearly be seen that there is a transient during the interval of 11.9 to 12 seconds. Nevertheless, the reader should not be deceived in the simplicity of detecting transients from the energy trace. Another plot of a transient behaviour will illustrate this better (refer to Fig. 16 (b)).

In Fig. 16 (b), the transition from the transient to the steady state is visible but only barely. However if one performs a linear least squares fit to the data, the amount of power dissipated in this case would be quite significantly underestimated. The results of such a calculation can actually be seen in Fig. 15 (d), where the lowest excitation for the 1.5 mm diameter particles for 45 Hz produced power dissipation results that underestimated what is measured in experiments. A better way to detect and filter the transients automatically is still being worked on. A promising indicator perhaps is the coordination number.

The coordination number is the ratio of number of contacts to the number of particles in the system. A plot of the evolution of the coordination number for the same system from Fig. 16 (b) is produced in Fig. 16 (c). The coordination number decays at an exponential rate, indicating that the clump is breaking up quickly with time. This shows that the coordination number is a far more sensitive transient indicator.

A plot of the percentage of power dissipation that involves friction is given in Fig. 17. Regardless of the amplitude of excitation and particle type, it is safe to say that all power dissipation in the configurations observed is dominated by friction.

The domination of friction leads to a simple hypothesis; if one could improve the conditions that lead to increased activities of attrition between the particles, damping efficiency would improve. A new set of power measurement experiments similar to those described in Section 3 were carried out; for a range of frequencies from 25 Hz and incrementally at every 20 Hz up to 225 Hz, and for a range of amplitudes from 5g and incrementally at 2g up to 17g. The height of the screw top lid was fixed at 0.9 cm, leaving almost no gap between the top surface of the particles and the lid. During operation, the particles rattle around in an almost stationary manner. A plot of the power dissipated is shown in Fig. 18 (a).

It can be seen that the power dissipated in this particular configuration is nearly 3 times that of the previous configuration with the same particle sizes and number. This lends partial credence to the hypothesis that particle damping efficiency is heavily dominated by friction. The plot of the damping loss factor (if we consider the particle agglomerates as an energy dissipating material) is shown in Fig. 18 (b). From the damping loss factor plot, peak damping seems to occur around 90 Hz between 14-17 g with a loss factor of around 0.2.

Simulations of the particle damping are then repeated using the same methodology as stated previously. The simulation for this wider range of frequencies and amplitudes will also allow one to ensure that the model holds well for different conditions. The plot of the power dissipation for the linear model with rigid walls can be seen in Fig. 18 (c). The portion of the power dissipated by friction is shown in Fig. 18 (d). It clearly shows the dominance of friction for all operation points, with it accounting for 70-75 percent of the power dissipated. It can be seen that the scale of power dissipated is similar to the levels seen in those measured from the experiments. However, the power dissipation level seems to be slightly lower at the lower frequencies and overestimated towards the higher frequencies (refer to Fig.18 (a)). The peak of power dissipation from simulations for equivalent amplitude levels also seems to occur at slightly higher frequencies compared to those acquired from the experiments.

The initial explanation for this discrepancy was assumed to be the inadequacy of the linear models in replicating the behaviour of the particles. An attempt to improvise on the model by using nonlinear models was performed to test this hypothesis. The nonlinear model used is the Hertz-Mindlin model [20], itself an approximation of the Mindlin-Deresiewicz model. It however does not reproduce the full continuous nonlinear shear properties of the original Mindlin-Deresiewicz model. It is chosen however as it is easy to implement in PFC3D and still reproduces some of the salient nonlinearities. The normal stiffness and the tangential stiffness of the model are given in Eqs. 36 and 37:

$$k_{ni} = \left(\frac{2G^* \sqrt{2R^*}}{3(1-\nu)} \right) \sqrt{\delta_n} \tag{36}$$

$$k_{si} = \left(\frac{2\left(\left(G^* \right)^2 3(1-\nu) R^* \right)^{1/3}}{2-\nu} \right) \tag{37}$$

Now if the simulations were repeated with associated parameters used in the linear models and with a Poisson's ratio of 0.3, the calculation of the energy dissipated is similar to that of the linear models (refer to Fig. 18 (e)). The percentage of power dissipated by friction (refer to Fig. 18 (f)) is also comparable to the linear models, albeit at a slightly higher level (between 76-81 percent). On one hand, this provides some verification that the linear model is constructed correctly; on the other hand, there is still no validation that the right model is constructed. Now this proves that either there are still other mechanisms that the current models fail to emulate, or the material properties were not estimated properly. The latter proposition is now explored with a very coarse form of sensitivity test. Due to the need to run a larger number of simulations for the sensitivity test, the initial positions of the particles prior to excitation is the same for all runs. All the other parameters of the models are also held constant with the exception of the variables that are to be tested for sensitivity.

If the coefficient of restitution (COR) is reduced to 0.3 (equivalent to 0.41 critical damping ratio for both particle-particle and particle-wall contacts) for the linear model (refer to Fig. 19 (a)), it is found that the results change considerably. In fact, the predictions are quite a close match to the experiments compared to the predictions calculated using the measured coefficient of restitution. The portion of power dissipation accounted by friction in this case is around 29-50 % in all cases (refer to Fig. 19 (b)). This is expected as collisional damping is dominant with this level of COR. If COR is increased to 0.65 (0.14 critical damping ratio), the power dissipation plot remains largely unchanged (refer to Fig. 19 (c)), with only a slight increase in power dissipation. The portion of dissipation accounted by friction can be seen to slowly edge upwards for all operating points, though collisional damping still dominates (refer to Fig. 19 (d)). As the COR is increased further to 0.825 (0.06 critical damping ratio), some qualitative differences emerge. The peak of power dissipation starts to get rounder and more power dissipation occurs over the higher frequencies (refer to Fig. 19 (e)). Power dissipation is also largely described by friction dissipation (refer to Fig. 19 (f)). The matching between the predictions of high COR and that of the experiments forces us to re-evaluate the supposed dominant role of friction. It is possible that the COR were overestimated as it does vary with impact velocity, and the increased levels of power dissipation from the previous configuration were from increased collision dissipation rather than friction attrition. Nonetheless, friction still plays a role in power dissipation and shall be examined next.

If the COR is reduced to 0, the portion of power dissipated by friction is 100 %. The power dissipation of such a configuration is shown in Fig. 20 (a). It can be seen that the power dissipation levels for such a configuration are still close to the experiments, although it has a lower peak and is skewed more towards the higher frequencies. If this configuration is juxtaposed with the predictions of a system with a COR of 0.92 and zero coefficient of friction (COF) (refer to Fig. 20 (b)), we can see that the latter matches up with the former in terms of power levels. Although the power of the zero friction system is heavily skewed towards the higher frequencies, it should be noted that the similar levels of dissipation are occurring for such a low collisional damping setting. When the coefficient of friction is varied to higher levels of 0.8 and 1.2, there appears to be almost no difference to the initial estimates (refer to Fig. 20 (c) and (e) respectively). The percentage of power accounted by friction also remains almost constant (refer to Figs. 20 (d) and (f)). It appears that this parameter is hard to alter from a design viewpoint and frictional dissipation may have to be encouraged from other methods, if it is to be encouraged at all.

A set of parameters that were not measured experimentally were the stiffness values. The values were approximated based on widely available material data, though it is possible that there may be variations between those values and what is used in practice. The stiffness of the particles is now varied to assess the impact of it on power dissipation. The normal stiffness was varied from a multiple of 0.01 to a multiple of 100 of the original stiffness for the linear models. Plots of the former and the latter are shown in Figs. 21 (a) and (c)

respectively. By reducing the stiffness estimates, the peak of the power dissipated have sharpened slightly. There is however still the overestimation of power dissipated for the higher frequency regions. The dissipation explained by friction is also about the same as the original approximation (refer to Fig. 21 (b)). Conversely, when the stiffness is increased a hundred fold, the peak of power dissipation drops, although power dissipated at the higher frequencies has increased. Friction dissipation has decreased significantly though (refer to Fig. 21 (d)). The effect of this stiffness variation may be part of the reason why there is discrepancy between the predictions and the measured power. One way this mismatch of stiffness can occur is when oxidation of some sort occurs at the particles, creating a softer external shell and decreasing the stiffness of the particles. The assumed stiffness values also play another role in a separate mechanism.

All the previous simulations make the assumption that the inner walls are rigid and the stiffness of the walls plays no role in terms of power dissipation. This is however obviously unrealistic as there is definitely compliance, especially for the case of stainless steel balls impacting a Perspex surface (stainless steel balls are relatively stiffer material wise). The stiffness of the walls for the linear models is adjusted to various multiples of the particle stiffness of decreasing stiffness and the simulations repeated to gauge the effect on power dissipation (refer to Figs. 22 (a) and (c)). It can be seen that as the stiffness of the walls are decreased to a factor of 1×10^{-2}, the power dissipated does not increase significantly. However, when the particle stiffness is decreased up to a level of 1×10^{-4} times of the particle stiffness, peak power dissipation have raised up to more than double those measured from experiments. Whether this can be realised in practice though is not known at the moment. Friction dissipation remains constant however in both cases.

The variations of the parameters based on engineering judgement seem to point towards a minimal influence of power dissipation by parameters that are directly related to friction, although it could still play an important role in damping. The stiffness does play a factor in the role of the power dissipated and shows that there is scope for further investigations. The most interesting aspect however, is that it seems collisional dissipation may play a more significant role in terms of the way power dissipation is attenuated over the different frequencies. Moreover, the interaction between all the different parameters may be nonlinear and the coarse sensitivity analysis may not be sufficient in terms of the domain tested.

6. Conclusion

The work reported in this paper aimed at finding more ways to better characterize a particle damper. The DEM technique used found reasonable correlation with the power dissipation calculated from an experiment. Predictions made using a linear model give largely similar results to those obtained assuming Hertz-Mindlin relationships. However, it must be stated that the method is very much in a developmental stage and discrepancies still exist between expected and predicted behaviour.

The work has shown that the dominant energy dissipation mechanism, based on the approximation of the material parameters, in the dampers studied is friction (responsible for 70% to 80% of power dissipation). Despite this being the case, the actual coefficient of friction has a minor effect on the dissipation characteristics. It appears however that as the coefficient of restitution decreases significantly below 0.9, its importance in the dissipation of energy increases. The simulations also show that large changes in contact stiffness of the particles and damper walls have an important effect on the power dissipated.

The simulations were also only performed in one realization. It is possible that the real system may be chaotic due to nonlinear mechanics and the random initial state in a multi particle system. More simulations would have to be perform, also for larger and more complicated contact mechanisms and geometry (such as irregular particle geometry, polydisperse particles etc.) to better understand other phenomena, such as convection, clustering, segregation and the momentum transfer mechanisms. With the DEM tool in hand, it will be interesting to attempt to optimize and possibly control particle dampers in a simulation. This would allow rapid prototyping of particle dampers while minimizing testing in the lab and the cost of manufacturing prototypes.

It is hoped that more experiments can be conducted in the future to further refine and verify these techniques. The characterization of the contact behaviour is at a crude level so far. Much work needs to be done to rectify this. More simulations with better sampling techniques could be used to assess the sensitivity and uncertainty the model has, as well as an extension of the initial tests done here, coupled together with some form of model updating method. Needless to say, despite all these advancements in computational and theoretical understanding, work so far has barely scratched the surface of the subject of granular media and its role in particle damping.

Acknowledgments

C.X. Wong is funded by EPSRC contract GR/T28393/01. The authors are grateful for the help extended by Dave Webster and Leslie Morton in setting up the experiment. The authors would also like to thank the anonymous reviewers for their constructive comments.

References

[1] J. A. Rongong and G. R. Tomlinson, Amplitude Dependent Behaviour in the Application of Particle Dampers to Vibrating Structures, *Proceedings of the Structural Dynamics & Materials Conference*, 2005.
[2] P. Lieber, and D. P. Jensen, An acceleration damper: Development, design, and some applications, *Transactions of the ASME*, 1945, pp. 523-530.

[3] H. V. Panossian, Structural damping enhancement via non-obstructive particle damping technique, *ASME Journal of Vibration and Acoustics* 114, 1992, pp 101-105.

[4] H. V. Panossian , Non-Obstructive Particle Damping: New Experiences and Capabilities, Proceedings of the 49th *AIAA/ASME/ASCE/AHS/ASC Structures, Structural Dynamics & Materials Conference,* 2008.

[5] C.Pendleton, J. P. Basile, J. E. Guerra, B. Tran, H. Ogomori and S. H. Lee, Particle Damping for Launch Vibration Mitigation: Design and Test Validation, *Proceedings of the 49th AIAA/ASME/ASCE/AHS/ASC Structures, Structural Dynamics & Materials Conference,* 2008.

[6] S. Simonian, V. Camelo, S. Brennan, N. Abbruzzese and B. Gualta, Particle Damping Applications for Shock and Acoustic Environment Attenuation, *Proceedings of the 49th AIAA/ASME/ASCE/AHS/ASC Structures, Structural Dynamics & Materials Conference, 2008*.

[7] N. Popplewell and M. Liao, A simple design procedure for optimum impact dampers, *Journal of Sound and Vibration* 146, No. 3, 1991, pp. 519-526.

[8] W. Liu, G.R. Tomlinson and J. A. Rongong, The dynamic characterisation of disc geometry particle dampers, *Journal of Sound and Vibration* 280, No. 3-5, 2005, pp. 849-861.

[9] V. K. Kinra, K. S. Marhadi and B. L. Witt., Particle Impact Damping of Transient Vibrations, *46th AIAA/ASME/ASCE/AHS/ASC Structures, Structural Dynamics & Materials Conference*, 2005.

[10] M. Y. Yang, Development of master design curves for particle impact dampers, Doctoral Thesis, The Pennsylvania State University, 2003.

[11] J. L. J. Driesen and R. J. M. Belmans, Wavelet-based power quantification approaches, *IEEE Transactions on Instrumentation and Measurement* 52, No. 4, Aug. 2003 ,pp. 1232 – 1238.

[12] C. Saluena, T. Poschel and S.E. Espiov, Dissipative properties of granular materials, *Physical Review E*, 59, 1999, pp. 4422-4425.

[13] I. Goldhirsch, Rapid Granular Flows, *Annual Review of Fluid Mechanics* 35, 2003, pp. 267-293.

[14] T. W. Martin, J. M. Huntley and R. D. Wildman, Hydrodynamic model for a vibrofluidized granular bed, *Journal of Fluid Mechanics* 535, 2005, pp. 325-345.

[15] T. Ohtsuki and T. Ohsawa, Hydrodynamics for Convection in Vibrating Beds of Cohesionless Granular Materials, *Journal of Physical Society of Japan* 72, No. 8, 2003, pp. 1963-1967.

[16] R. M. Nedderman, *Static and kinematics of granular materials*, Cambridge University Press, Cambridge, U.K., 1992.

[17] P. Jop, Y. Forterre and O. Pouliquen, A constitutive law for dense granular flows, *Nature* 441, 2006, pp. 727-730.

[18] S. Dartevelle, Numerical and granulometric approaches to geophysical granular flows, Ph.D. thesis, Michigan Technological University, Department of Geological and Mining Engineering, Houghton, Michigan, July 2003.

[19] H. J. Herrmann and S. Luding, Modeling granular media on the computer, *Contin. Mech. Thermodyn*. 10, 1998, pp. 189-231.

[20] P. A. Cundall, *Computer Simulations of Dense Sphere Assemblies, Micromechanics of Granular Materials*, Satake. M. and Jenkins, J.T., Eds. Amsterdam: Elsevier Publishers, B. V., 1988, pp. 113-123.

[21] K. Mao, M. Y. Wang, Z. Xu and T. Chen, Simulation and Characterization of Particle Damping in Transient Vibrations, *Journal of Vibration and Acoustics* 126, No. 2, 2004, pp. 202-211

[22] R. D. Wildman, J. P. Huntley and D. J. Parker, Convection in highly fluidized three-dimensional granular beds, *Phys. Rev. Lett.* Vol. 86, 2001, pp. 3304-3307.

[23] Itasca Consulting Group Inc., UDEC (Universal Distinct Element Code), Version 4.0. Minneapolis:ICG, 2004.

[24] K. L. Johnson, *Contact Mechanics*, Cambridge University Press, Cambridge 1985.

[25] W. J. Stronge, *Impact Mechanics*, Cambridge University Press, 2000.

[26] J. Coaplen, W. J. Stronge and B. Ravani, Work Equivalent Composite Coefficient of Restitution, *International Journal of Impact Engineering* 30, No. 6, 2004.

[27] C. X. Wong, M. C. Daniel, and J. Rongong, Prediction of the amplitude dependent behaviour of particle dampers, *48th AIAA/ASME/ASCE/AHS/ASC Structures, Structural Dynamics & Materials Conference*, 2007.

[28] R. D. Mindlin and H. Deresiewicz, Elastic Spheres in Contact under Varying Oblique Forces, *Journal of Applied Mechanics* 20, 1953, pp. 327-344.

[29] T. Kawaguchi, Numerical Simulation of Fluidized Bed Using the Discrete Element Method (the Case of Spouting Bed), *JSME (B)* 58, No. 551, 1992, pp. 79-85.

[30] S. McNamara and E. Falcon, Simulations of vibrated granular medium with impact-velocity-dependent restitution coefficient, *Physical Review E* 71, No. 3, id 031302, 2005.

[31] T. Belytschko, An Overview of Semidiscretization and Time Integration Procedures, Computational Methods for Transient Analysis, Ch. 1. T. Belytschko and T. J. R. Hughes, Eds. New York: Elsevier Science Publishers, B. V., 1983, pp. 1-65.

[32] C. X. Wong, Nonlinear System Identification with Emphasis on Dry Friction, Ph.D. thesis, University of Sheffield, Department of Mechanical Engineering, Sheffield, U.K., September 2005.

[33] Y. Li, Y. Xu and C. Thornton, A comparison of discrete element simulations and experiments for sandpiles composed of spherical particles, *Powder Technology* 160, 2005, pp. 219 – 228.

List of Figures

Fig. 14. DEM simulation of the particle damper with 1800 particles of 1.5 mm diameter during (a) particle generation process, (b) particles in the "settled" state and (c) particles during excitation.

Fig. 15. Comparison of power dissipation measured from experiments and that from simulations (a) 225 particles with diameter of 3.0 mm, (b) 360 particles with diameter of 2.5 mm, (c) 789 particles with diameter of 2.0 mm, (d) 1800 particles with diameter of 1.5 mm..

Fig. 16. Transient behaviour in the energy trace for (a) energy dissipated in a system with 225 particles, 3mm diameter at 45 Hz and 13g, (b) energy dissipated in a system with 1800 particles, 1.5 mm diameter at 5g, (c) coordination number in a system with 1800 particles, 1.5 mm diameter at 5g.

Fig. 17. Percentage of power dissipated by friction for various configurations (a) 225 particles of 3.0 mm diameter, (b) 360 particles of 2.5 mm diameter, (c) 789 particles of 2.0 mm diameter, (d) 1800 particles of 1.5 mm diameter.

Fig. 18. Power dissipation results for 225 particles of 3.0 mm diameter (a) power measured from experiments, (b) damping loss factor measured from experiment, (c) power dissipation predictions from linear model, (d) percentage of power dissipated by friction for linear model, (e) power dissipation predictions from Hertz-Mindlin model. (f) percentage of power dissipated by friction for Hertz-Mindlin model.

Fig. 19. Power dissipation prediction of linear models for 225 particles of 3.0 mm diameter (a) COR of 0.3 (particle-particle and particle-wall) for linear model, (b) percentage explained by friction (COR of 0.3), (c) COR 0.65 (particle-particle and particle-wall) for linear model, (d) coefficient of friction of 0 (particle-particle) for Hertz-Mindlin model, (e) coefficient of friction of 0.8 (particle-particle), (f) coefficient of friction of 1.2 (particle-particle) for Hertz-Mindlin model.

Fig. 20. Power dissipation prediction of linear models for 225 particles of 3.0 mm diameter (a) power dissipated by friction only, (b) no friction present, (c) COF of 0.8, (d) percentage of power explained by friction (COF of 0.8), (e) COF of 1.2, (f) percentage of power explained by friction (COF of 1.2)..

Fig. 21. Power dissipation prediction of linear models for 225 particles of 3.0 mm diameter (a) particle stiffness decreased by a factor of 0.01, (b) percentage of power explained by friction (particle stiffness decreased by a factor of 0.01), (c) particle stiffness increased by a factor of 100, (d) percentage of power explained by friction (particle stiffness increased by a factor of 100)

Fig. 22. Power dissipation prediction of linear models for 225 particles of 3.0 mm diameter (a) stiffness of walls set to 1 x 10^{-2} times the particle stiffness (b) percentage of power explained by friction (stiffness of walls set to 1 x 10^{-2} times the particle stiffness), (c) stiffness of walls set to 1 x 10^{-4} times the particle stiffness, (d) percentage of power explained by friction (stiffness of walls set to 1 x 10^{-4} times the particle stiffness).

List of Tables

Fig 1

Click here to download high resolution image

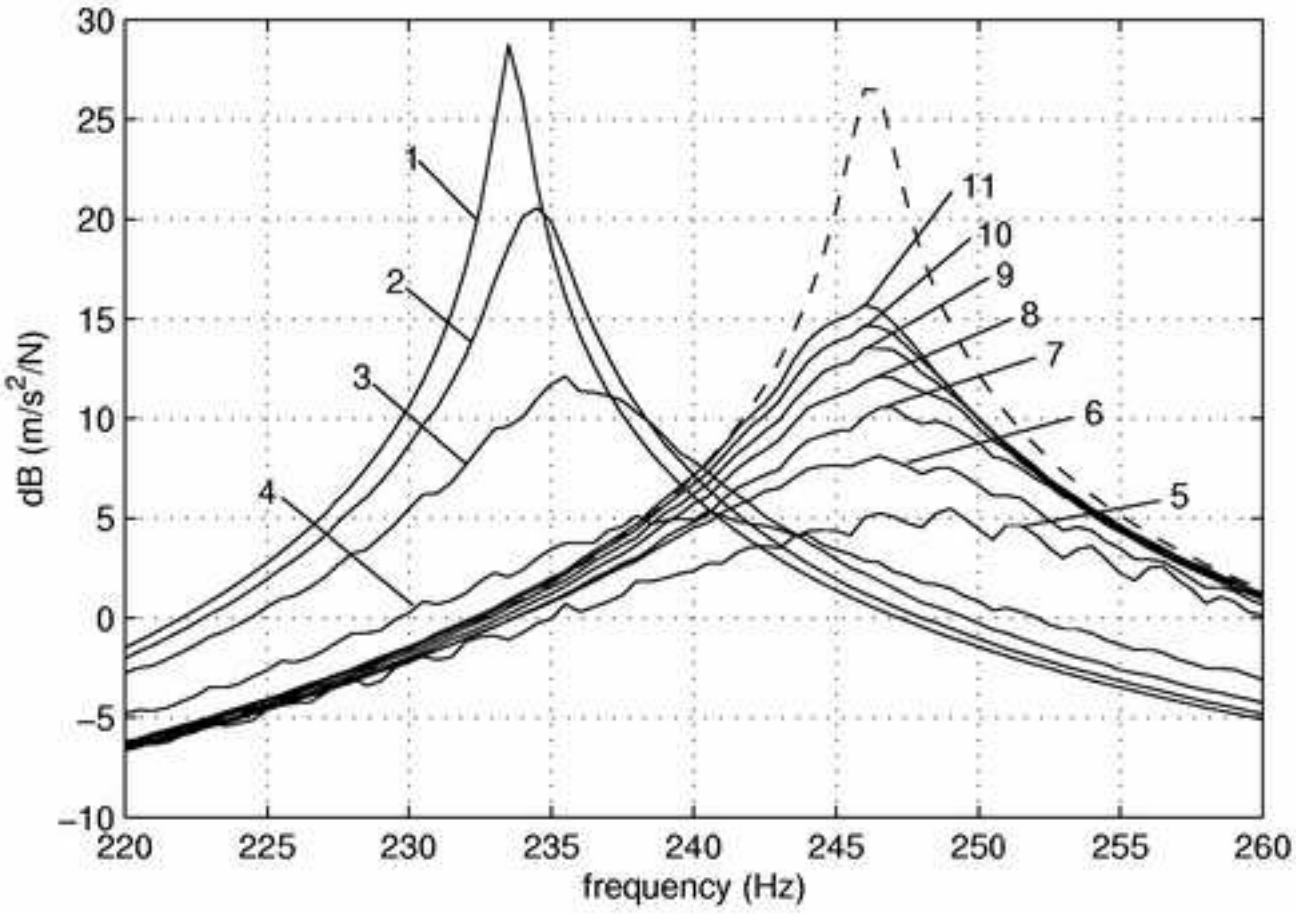

Fig 2

Click here to download high resolution image

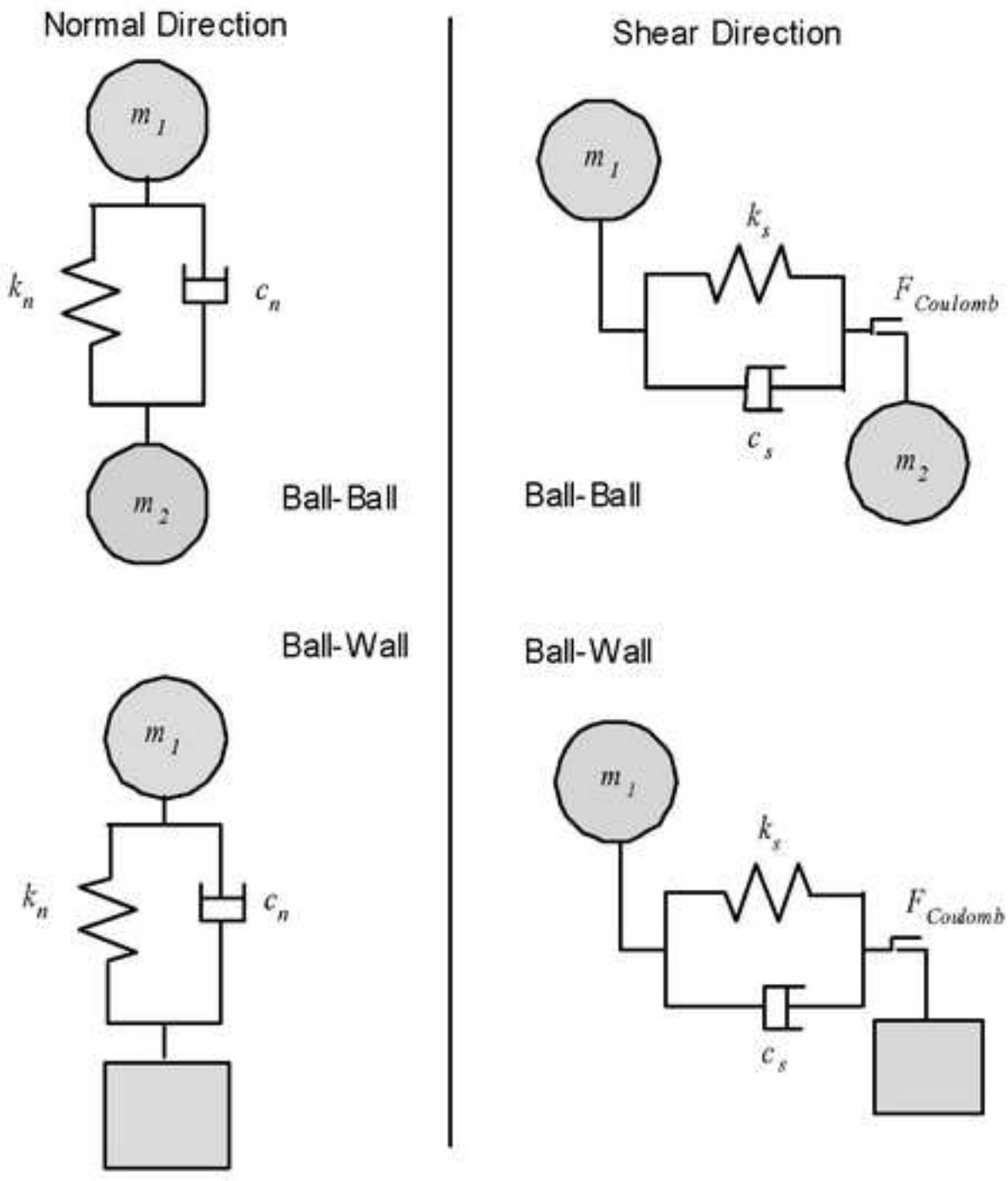

Fig 3

Click here to download high resolution image

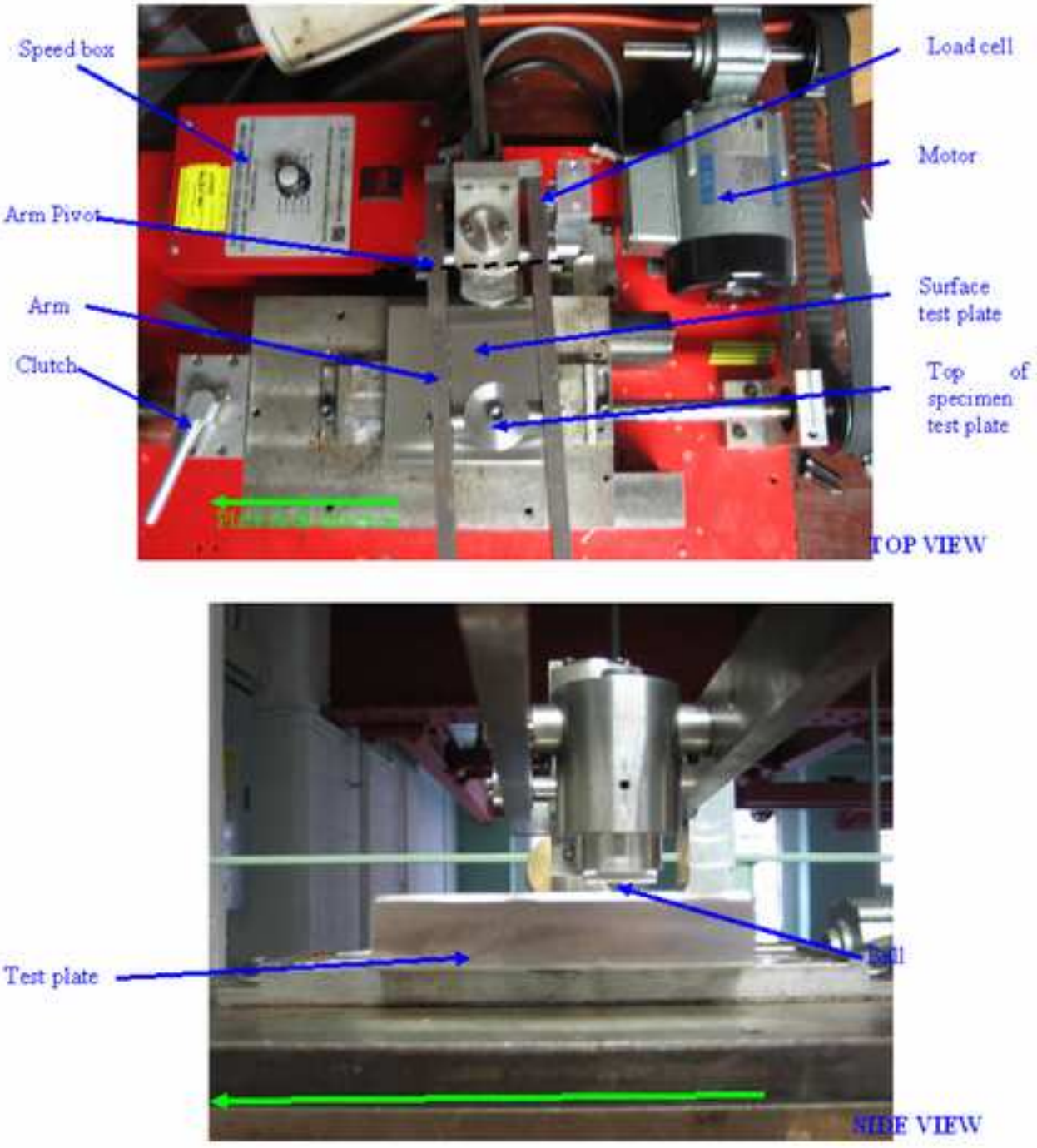

Fig 4

Click here to download high resolution image

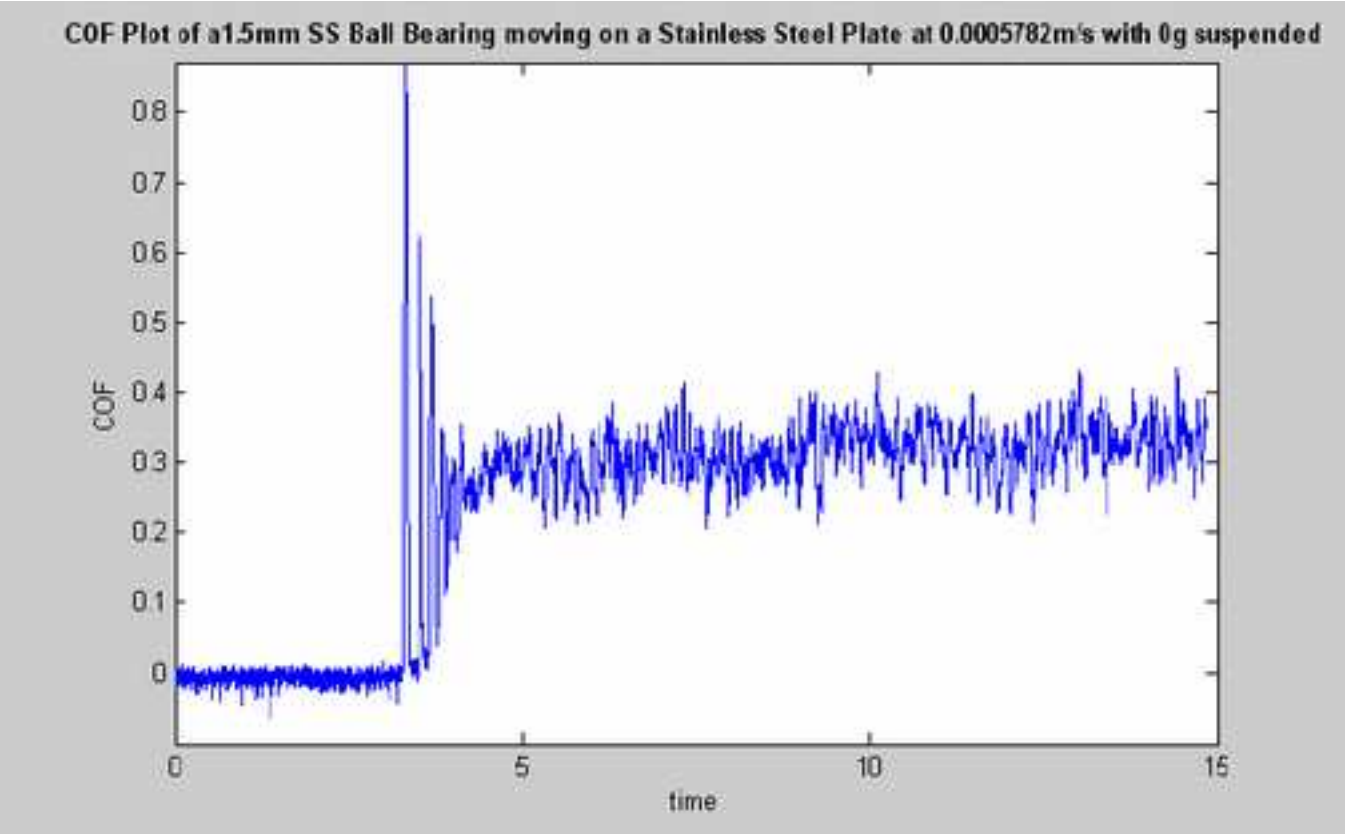

Fig 5

Click here to download high resolution image

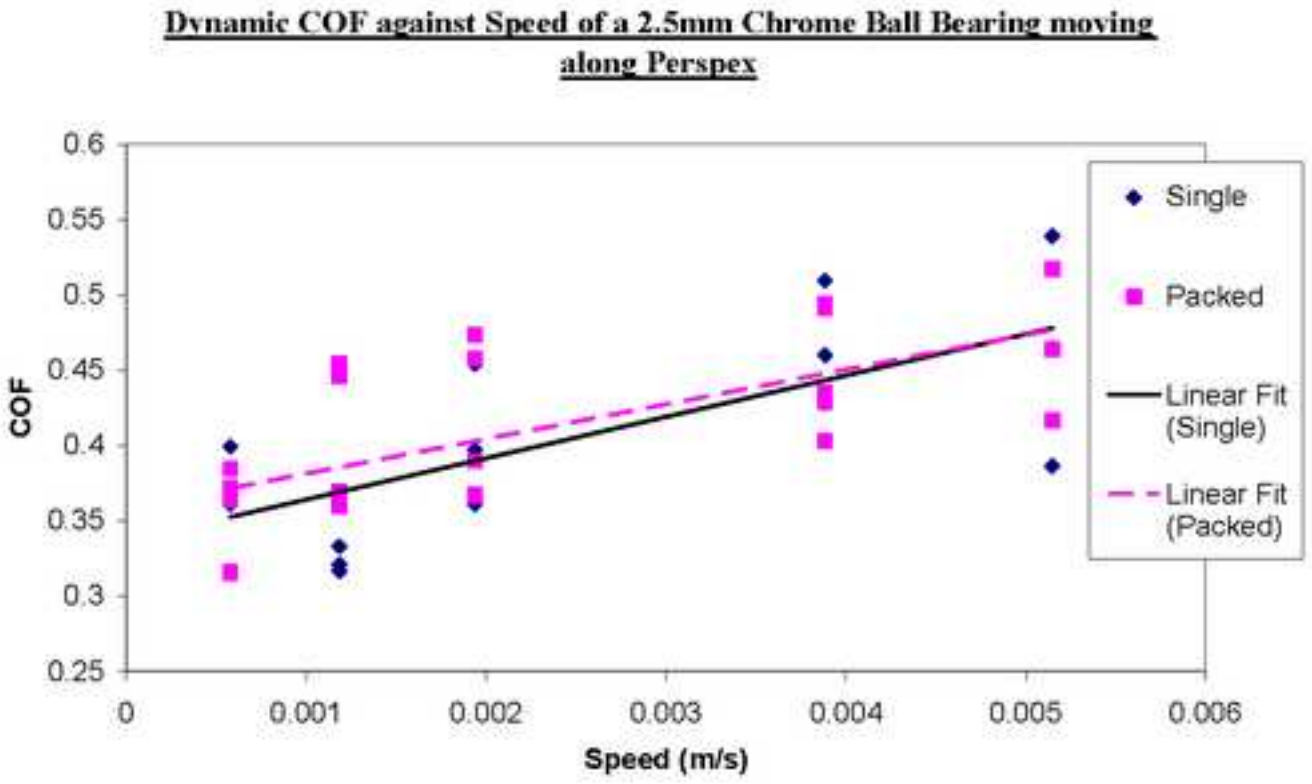

Fig 6

Click here to download high resolution image

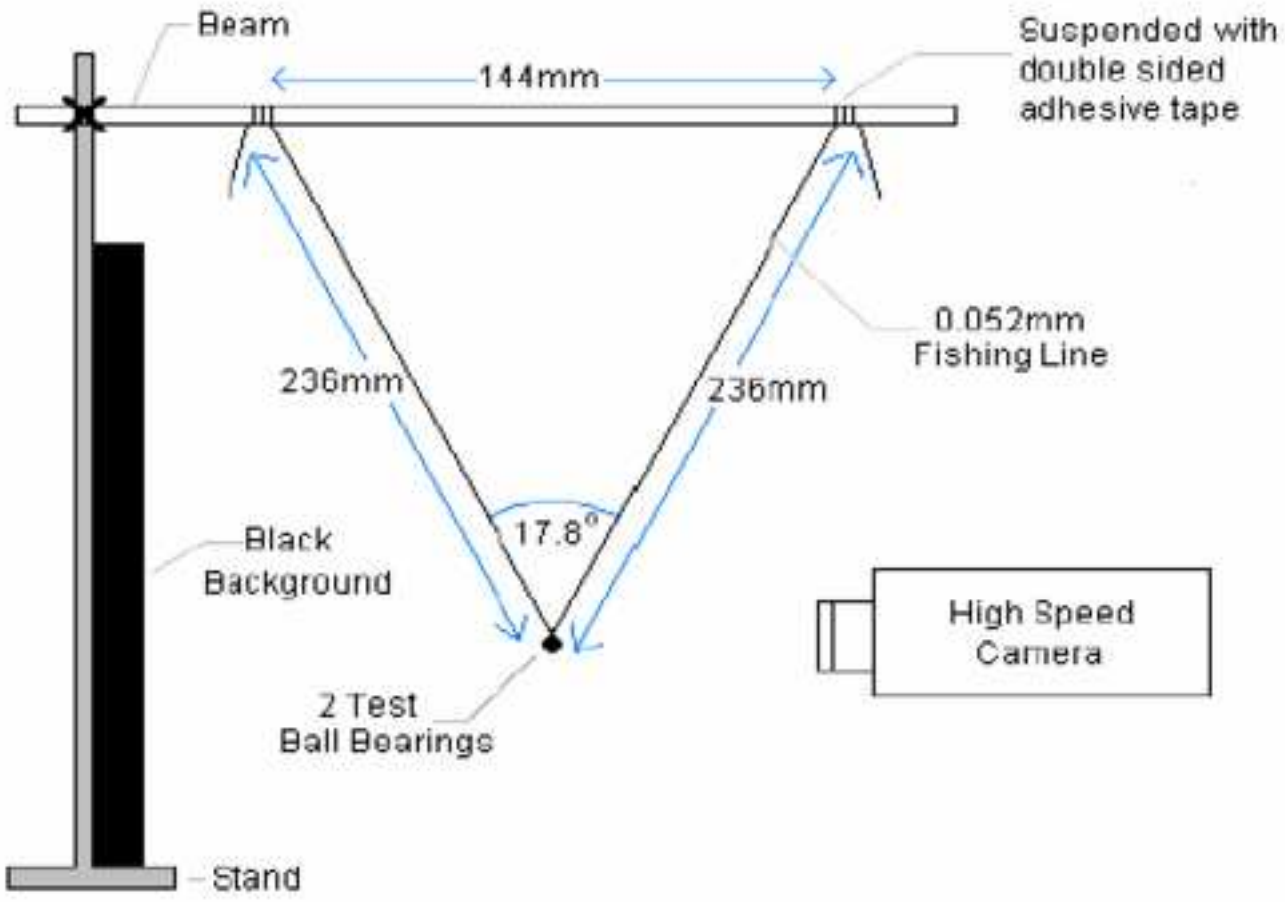

Fig 7

Click here to download high resolution image

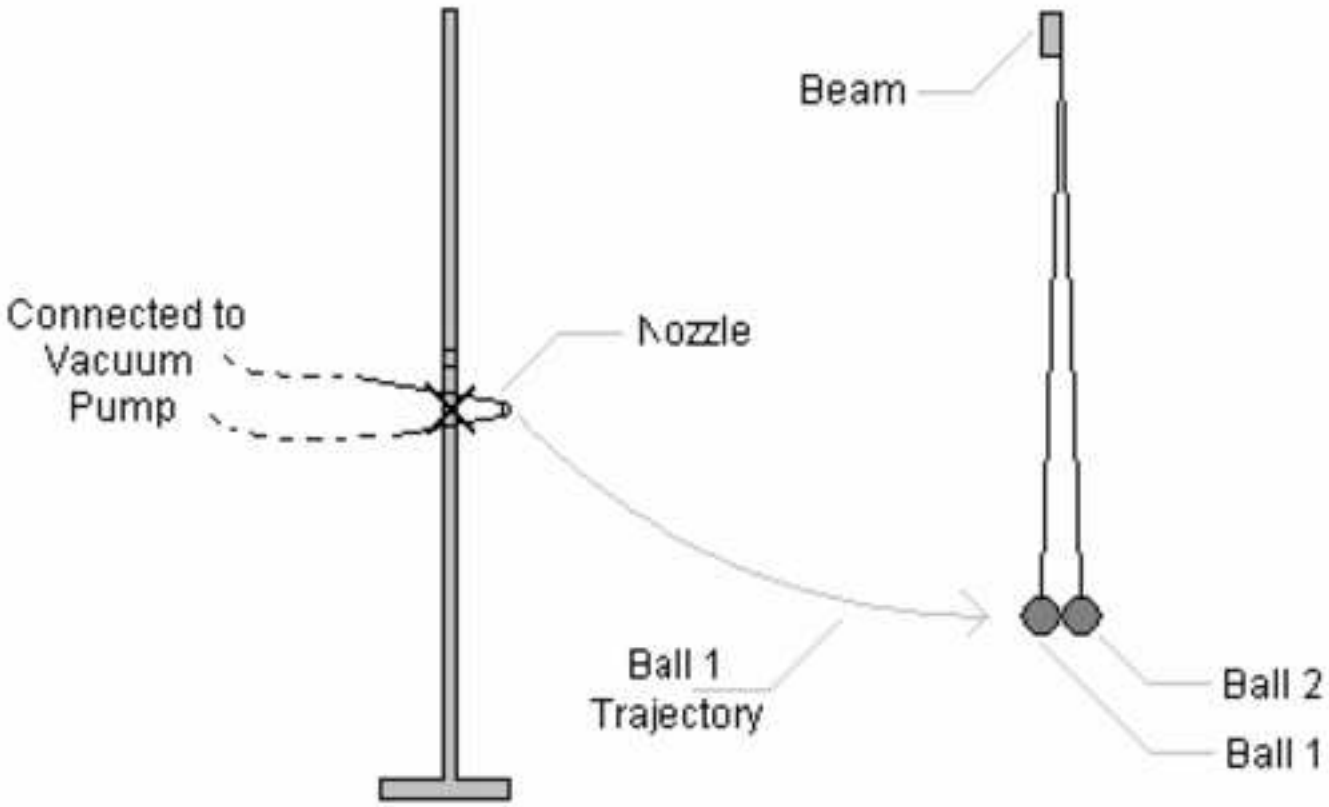

Fig 8

Click here to download high resolution image

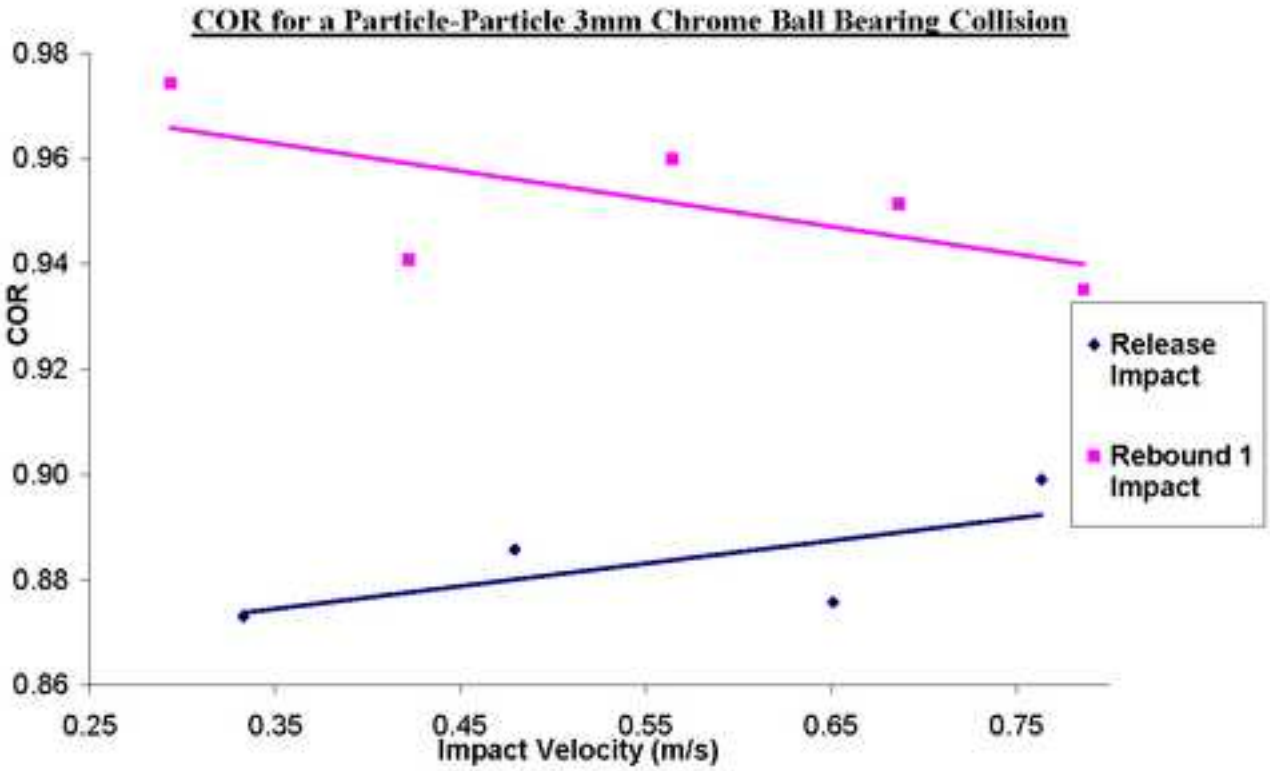

Fig 9

Click here to download high resolution image

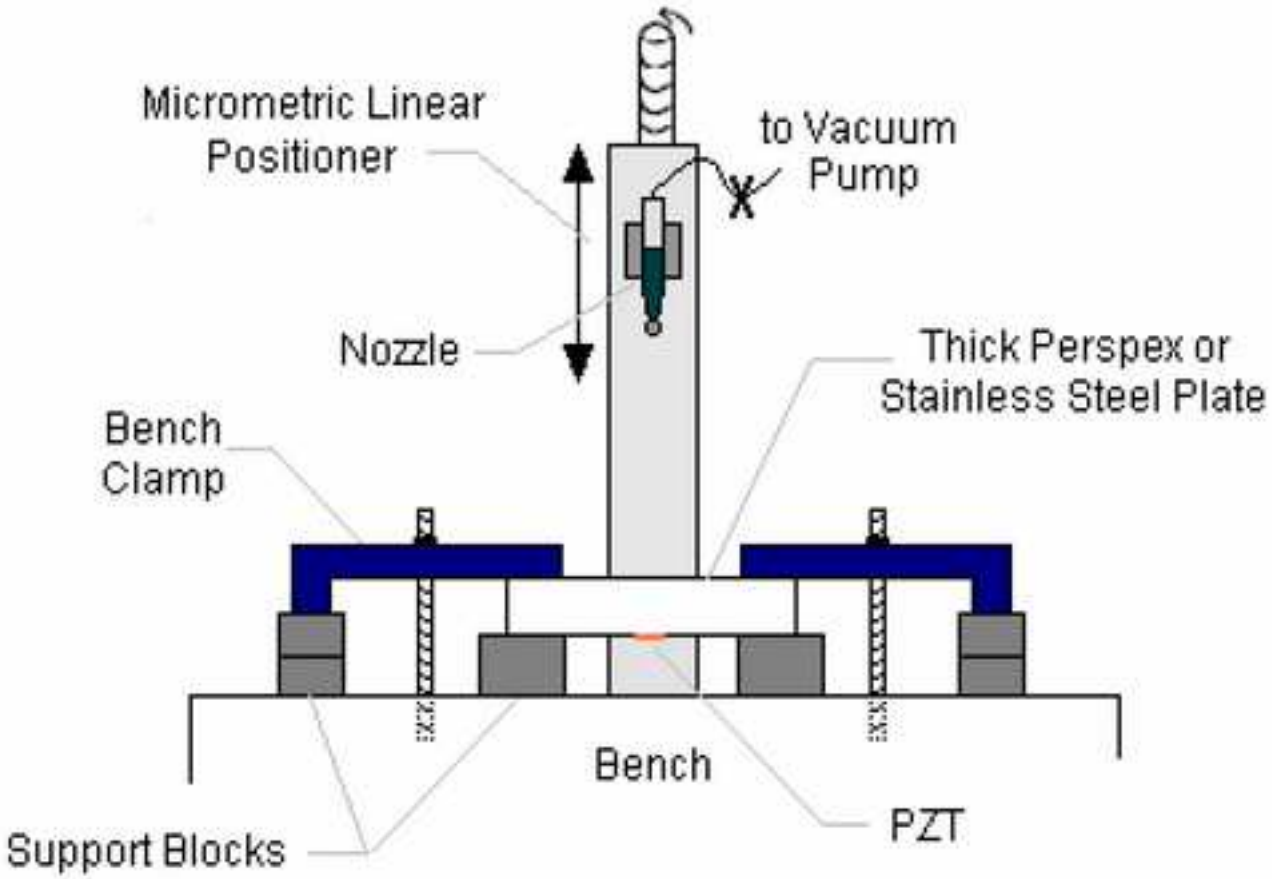

Fig 10

Click here to download high resolution image

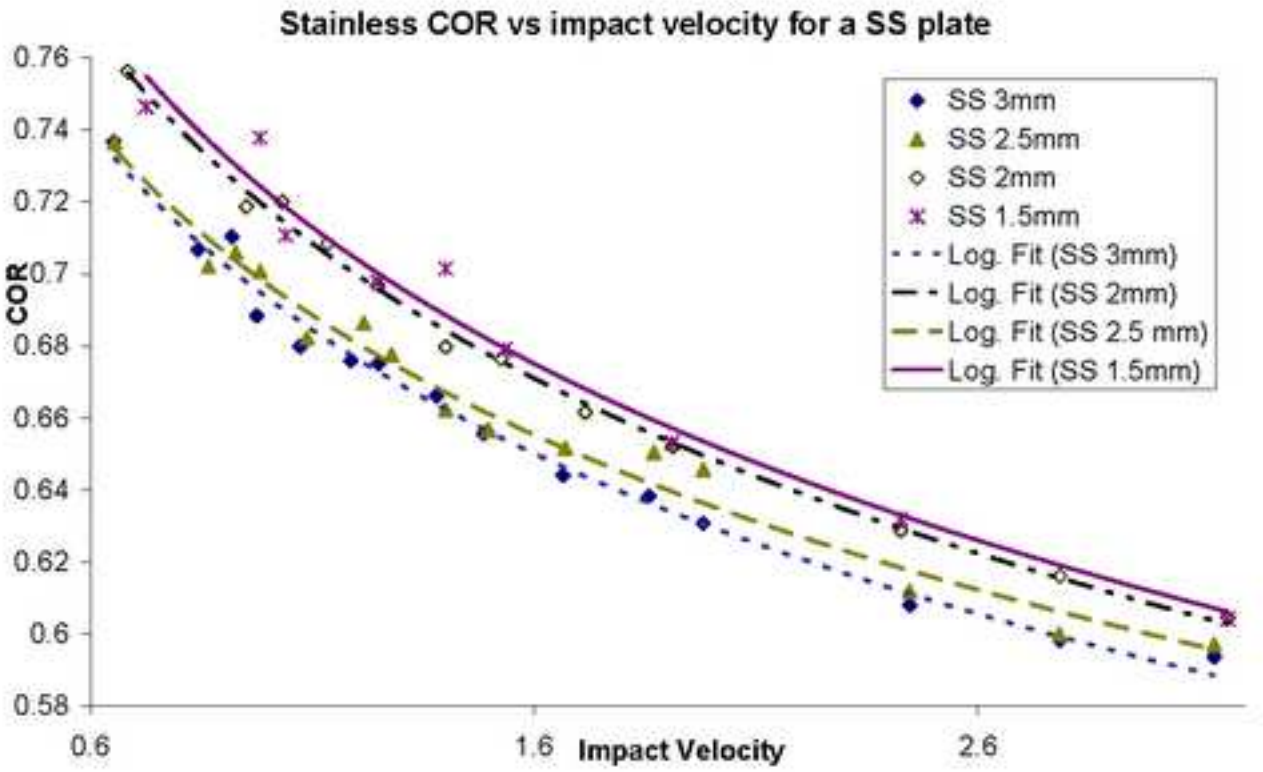

Fig 11

Click here to download high resolution image

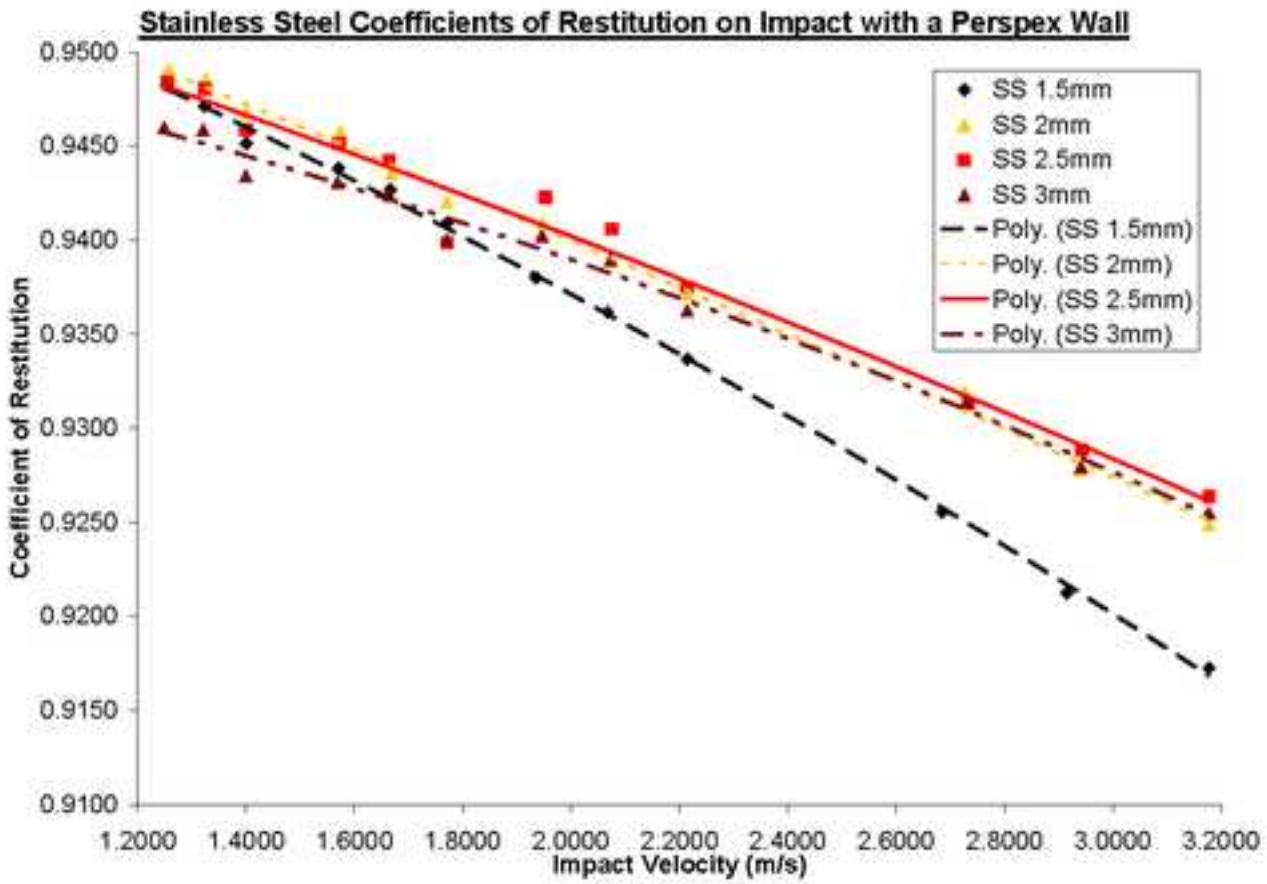

Fig 12

Click here to download high resolution image

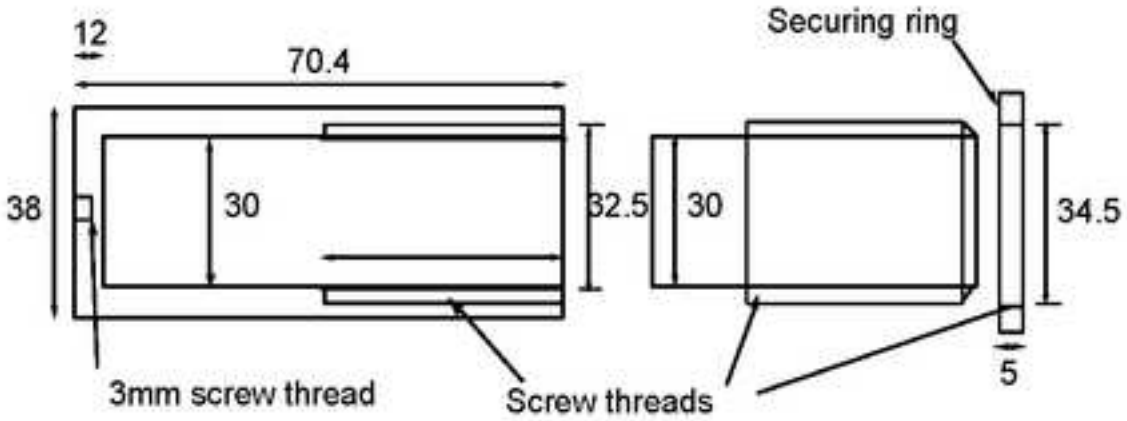

Fig 13

Click here to download high resolution image

Fig 14

Click here to download high resolution image

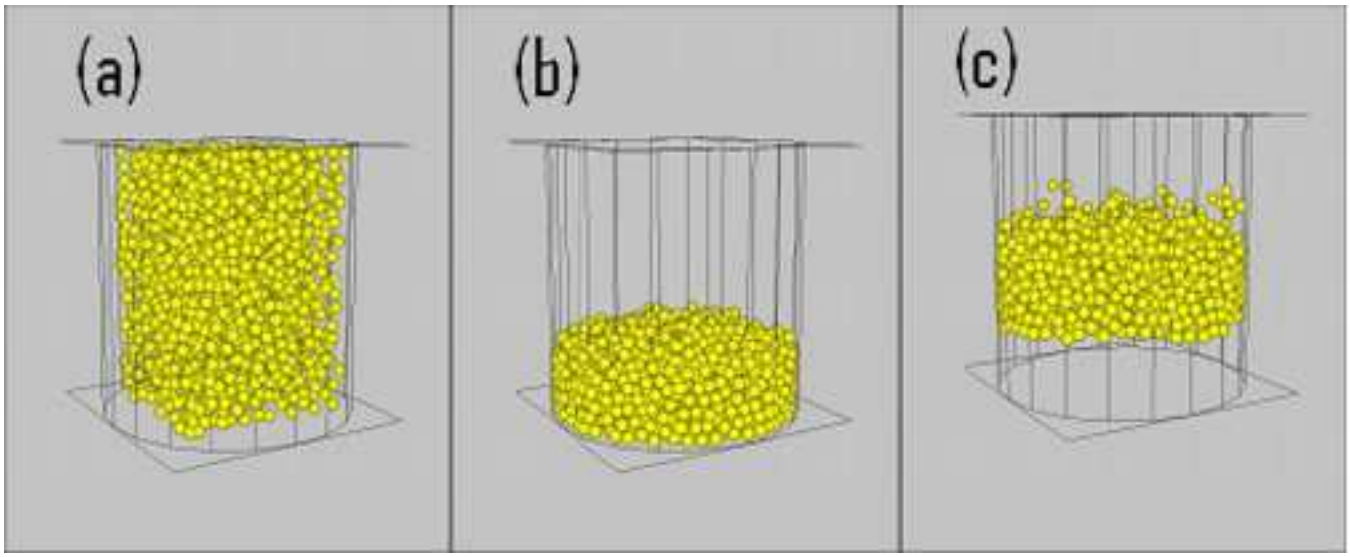

Fig 15

Click here to download high resolution image

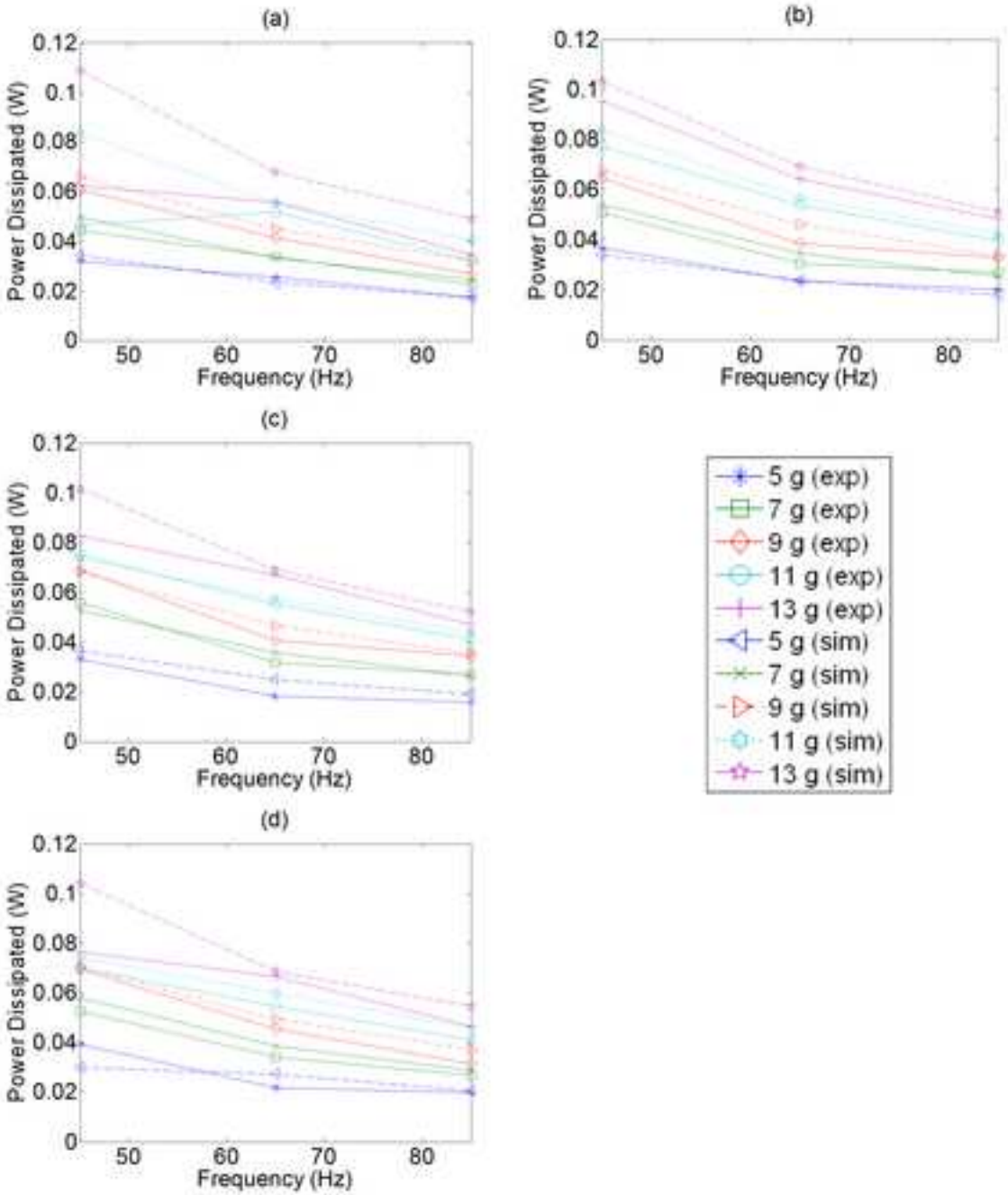

Fig 16

Click here to download high resolution image

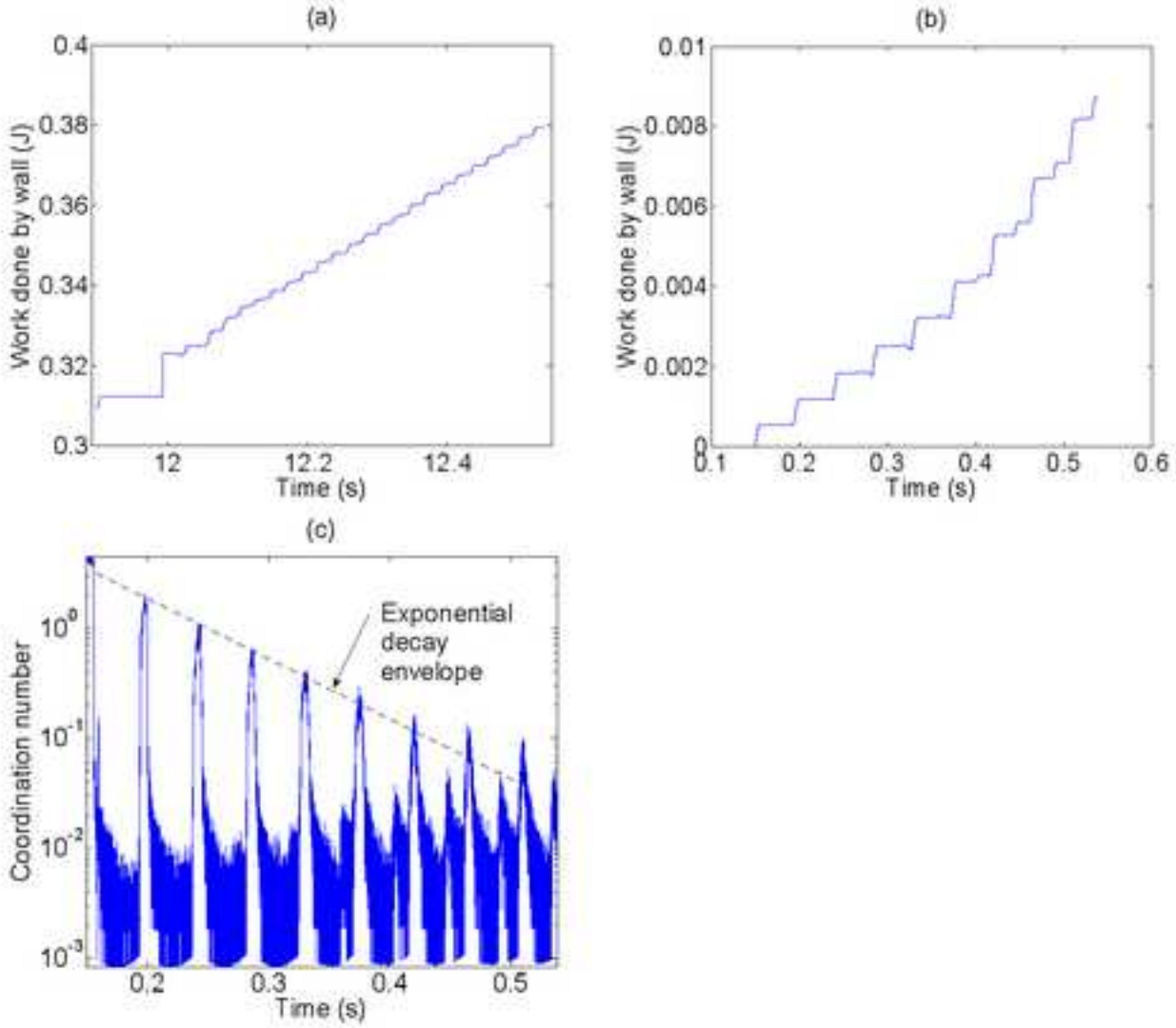

Fig 17

Click here to download high resolution image

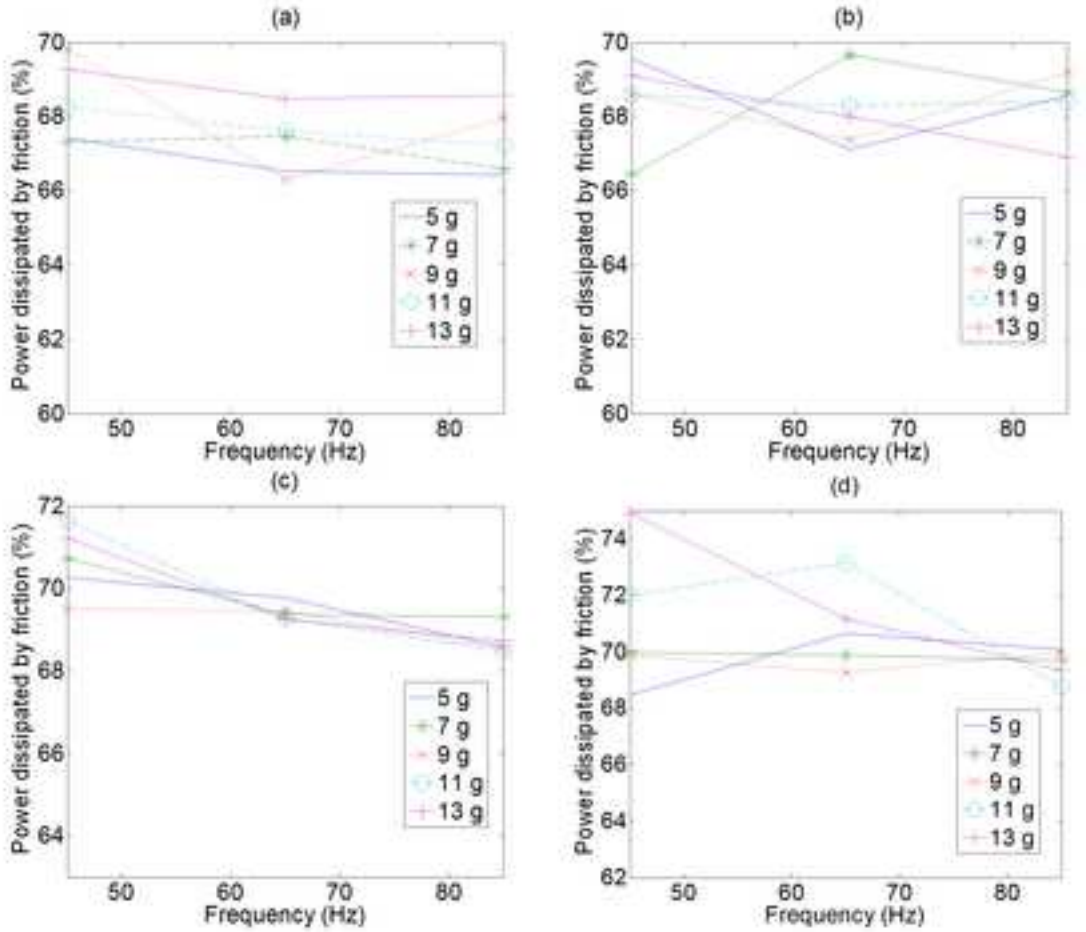

Fig 18

Click here to download high resolution image

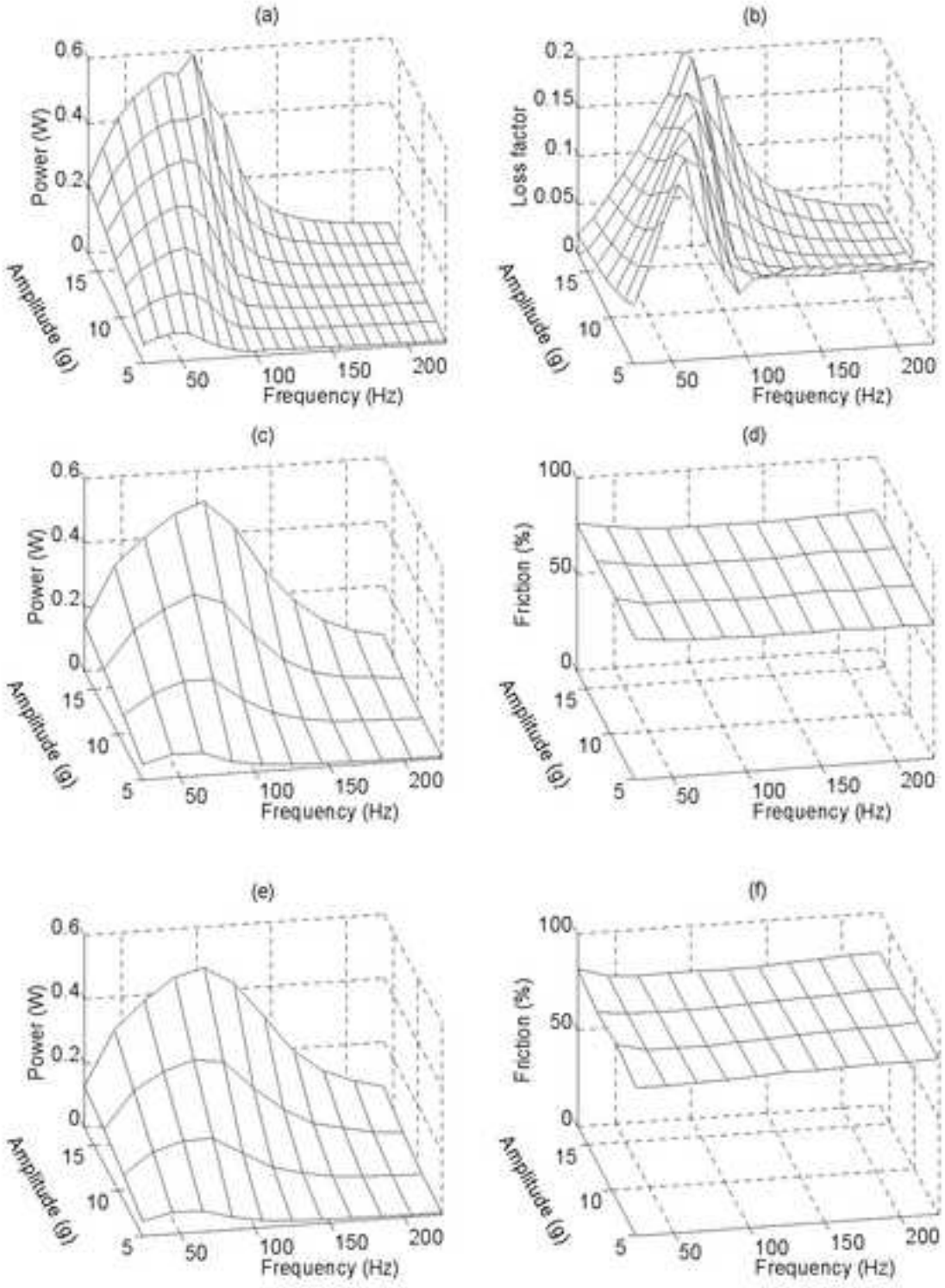

Fig 19

Click here to download high resolution image

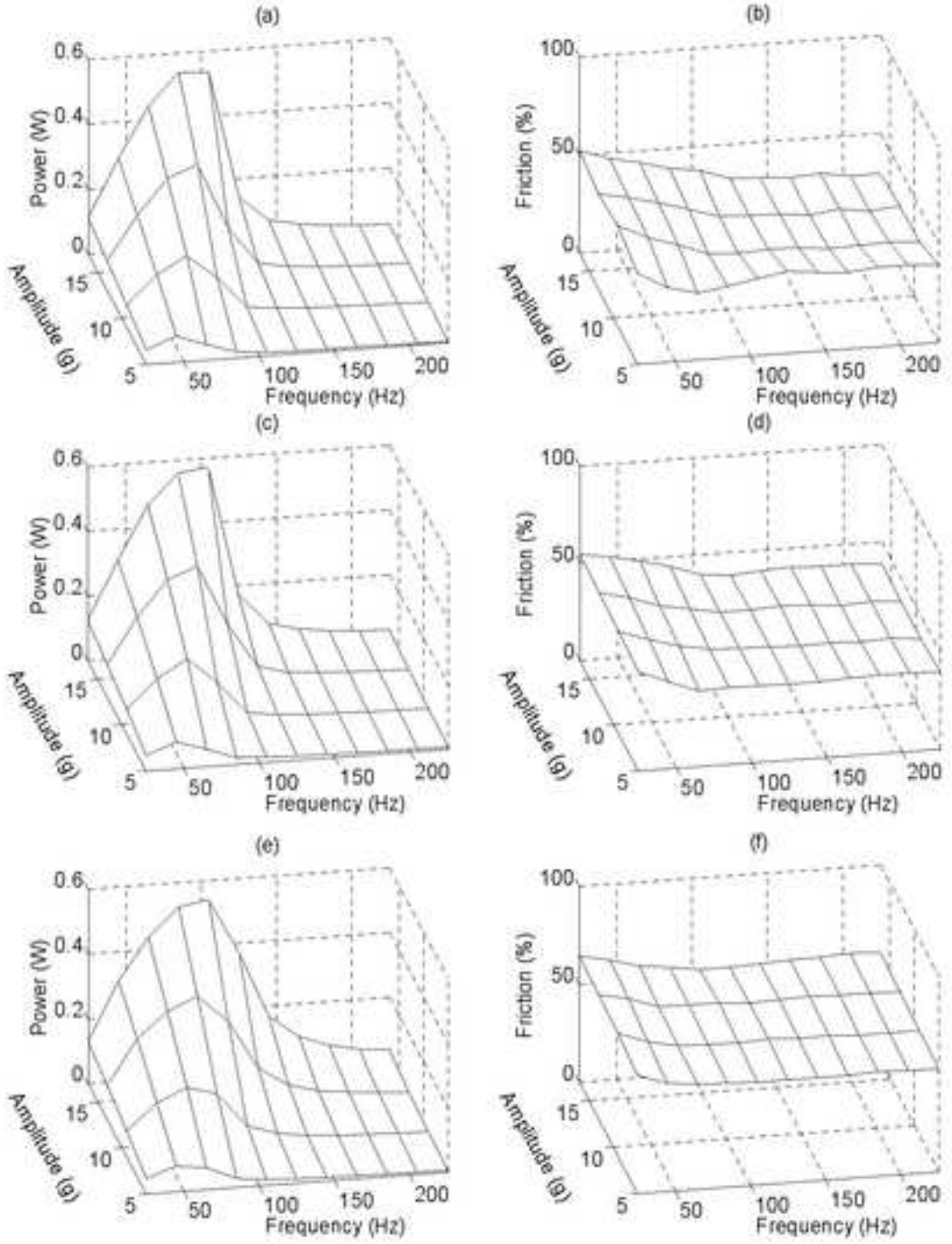

Fig 20

Click here to download high resolution image

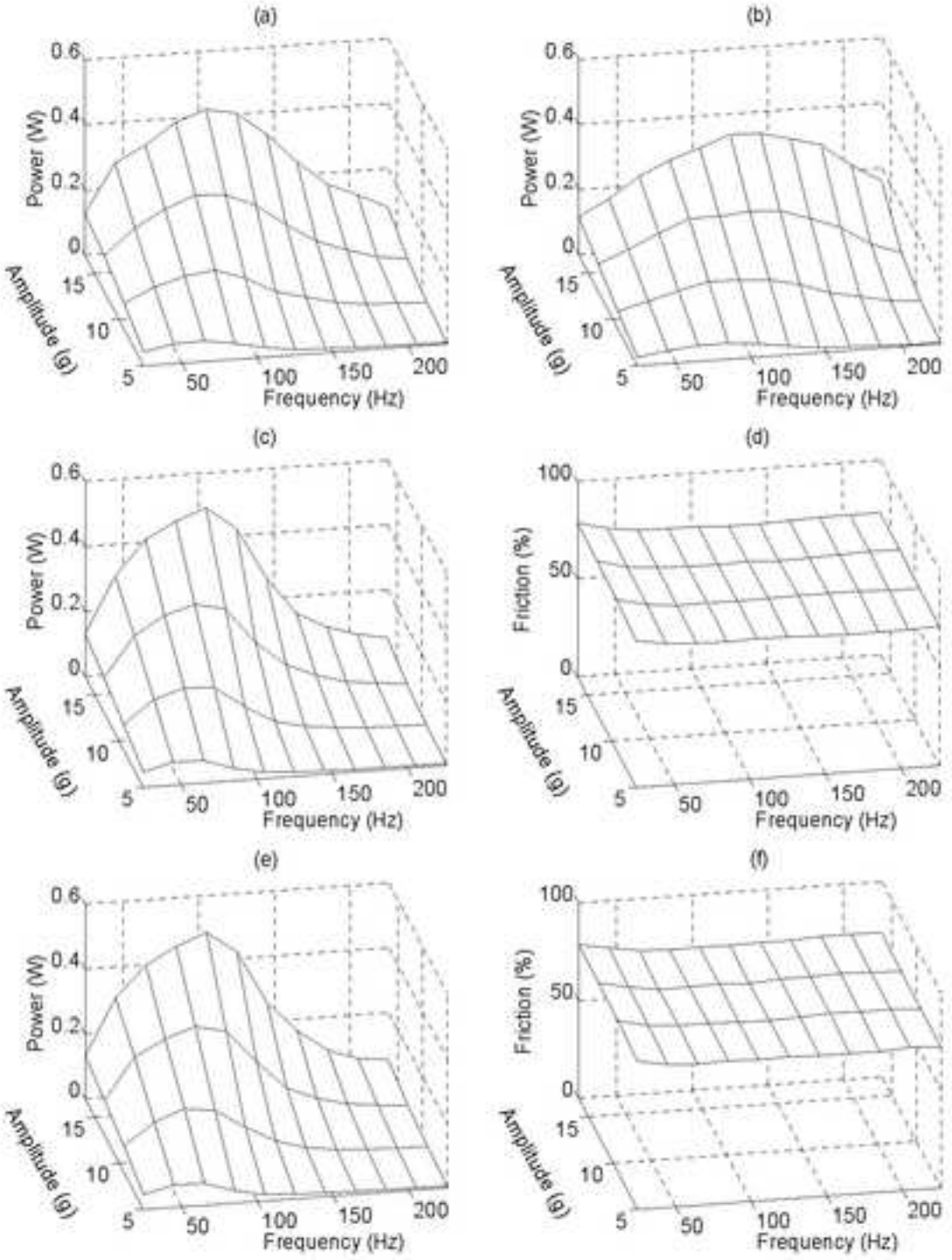

Fig 21

Click here to download high resolution image

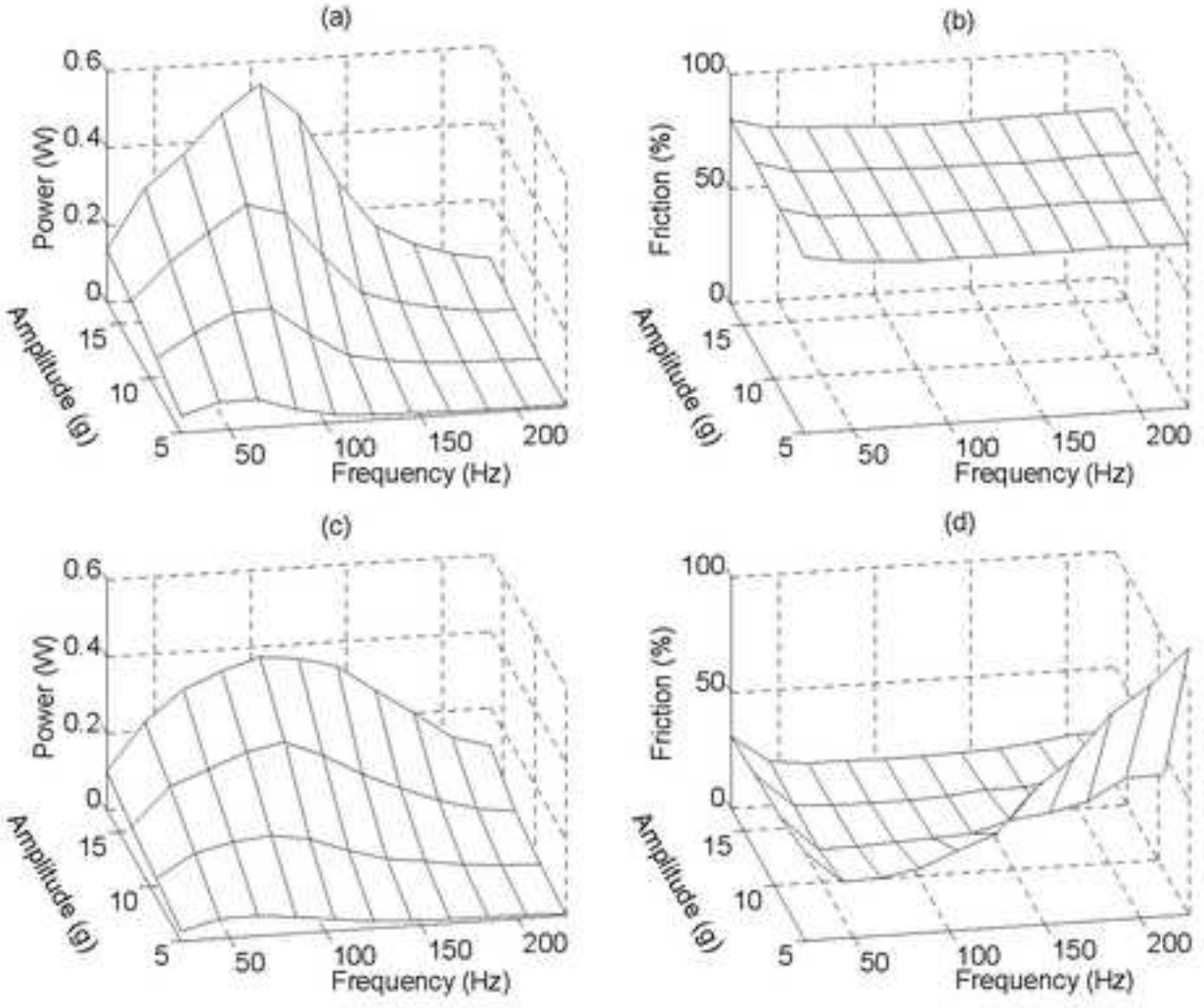

Fig 22
Click here to download high resolution image

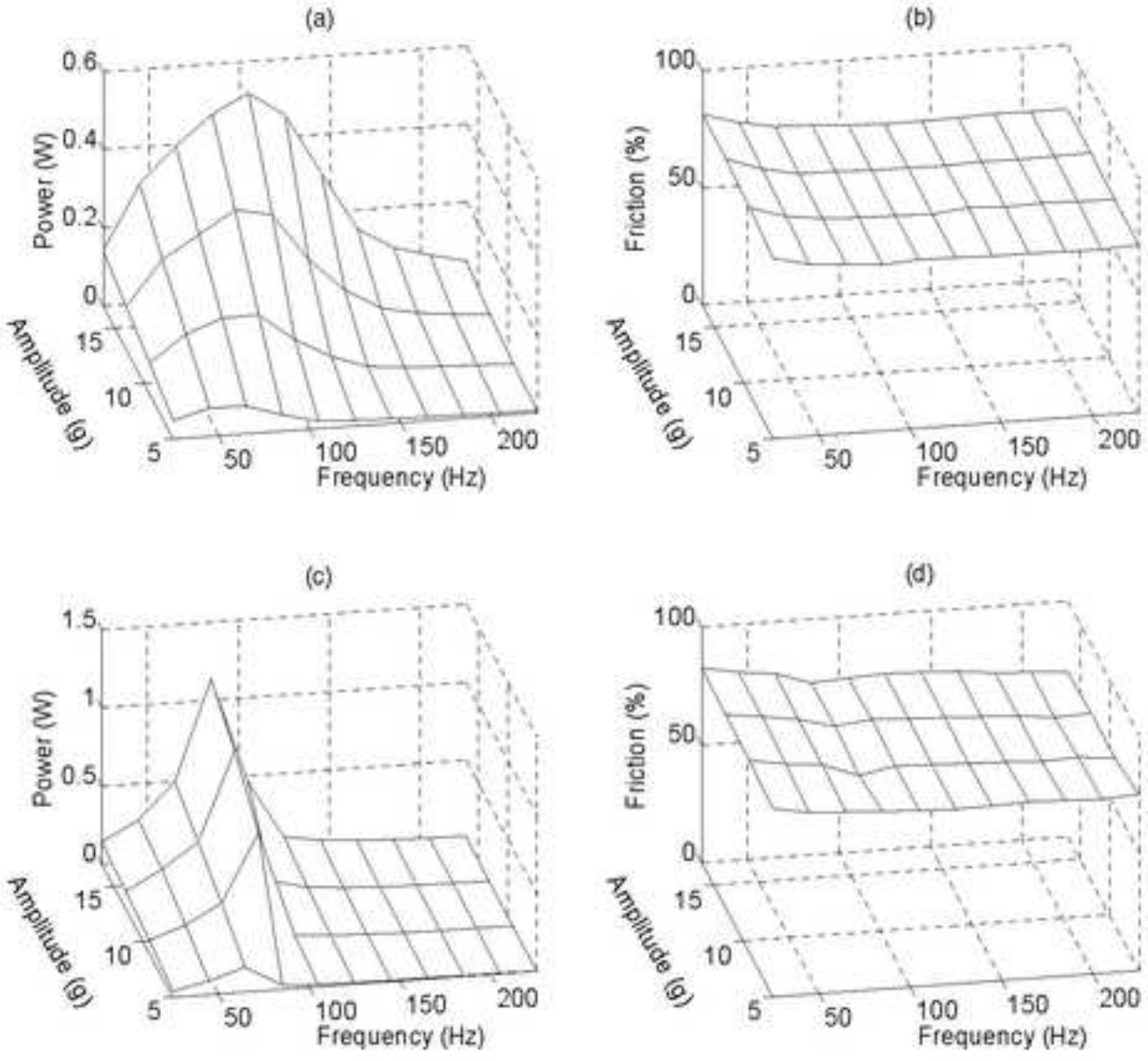

Table 1

Click here to download high resolution image

SUMMARY	Stainless Steel Test Plate - against the grain		Stainless Steel Test Plate - with the grain		Perspex Test Plate	
Ball Type	Gear 2 (0.0005782m/s)	Gear 6 (0.0038843m/s)	Gear 2 (0.0005782m/s)	Gear 6 (0.0038843m/s)	Gear 2 (0.0005782m/s)	Gear 6 (0.0038843m/s)
0.6mm SS shot	0.4616	0.5762	0.4007	-	0.4106	-
1.5mm Chrome	0.3214	0.3670	0.2906	-	0.3826	-
1.5mm SS	0.3076	0.4106	0.3550	-	0.3429	0.3152
3mm Chrome	0.3236	0.3942	0.2635	-	0.3968	0.3919
3mm SS	0.2651	0.4159	0.2849	-	0.4238	0.4594